


12-2014

Fabrication and Characterization of Magnetic Nanoparticle Composite Membranes

Akeem Cruickshank

Clemson University, acruick@g.clemson.edu

Follow this and additional works at: https://tigerprints.clemson.edu/all_theses

 Part of the [Materials Science and Engineering Commons](#), and the [Nanoscience and Nanotechnology Commons](#)

Recommended Citation

Cruickshank, Akeem, "Fabrication and Characterization of Magnetic Nanoparticle Composite Membranes" (2014). *All Theses*. 2062.
https://tigerprints.clemson.edu/all_theses/2062

This Thesis is brought to you for free and open access by the Theses at TigerPrints. It has been accepted for inclusion in All Theses by an authorized administrator of TigerPrints. For more information, please contact kokeefe@clemson.edu.

FABRICATION AND CHARACTERIZATION OF MAGNETIC NANOPARTICLE
COMPOSITE MEMBRANES

A Thesis
Presented to
the Graduate School of
Clemson University

In Partial Fulfillment
of the Requirements for the Degree
Master of Science
Materials Science and Engineering

by
Akeem Armand Cruickshank
December 2014

Accepted by:
Dr. M. S. Kennedy, Committee Co-Chair
Dr. O. T. Mefford, Committee Co-Chair
Dr. E. Skaar

ABSTRACT

To effectively and accurately deliver drugs within the human body, both new designs and components for implantable micropumps are being studied. Designs must ensure high biocompatibility, drug compatibility, accuracy and small power consumption. The focus of this thesis was to fabricate a prototype magnetic nanoparticle membrane for eventual incorporation into a biomedical pump and then determine the relationship between this membrane deflection and applied pneumatic or magnetic force. The magnetic nanoparticle polymer composite (MNPC) membranes in this study were composed of crosslinked polydimethylsiloxane (PDMS) and iron oxide nanoparticles (IONPs). An optimal iron oxide fabrication route was identified and particle size in each batch was approximately 24.6 nm. Once these nanoparticles were incorporated into a membrane (5 wt. %), the nanoparticle formed agglomerates with an average diameter of $2.26 \pm 1.23 \mu\text{m}$. Comparisons between the 0 and 5 wt. % loading of particles into the membranes indicated that the elastic modulus of the composite decreased with increasing particle concentration. The pressure- central deflection of the membranes could not be predicated by prior models and variation between magnetic and pneumatic pressure-deflection curves was quantified. Attempts to fabricate membranes with above 5 wt. % nanoparticles were not successful (no gelation). Fourier Transform Infrared (FTIR) spectroscopy results suggest that excess oleic acid on the nanoparticles prior to mixing might have prevented crosslinking.

ACKNOWLEDGMENTS

First and foremost, I would like to thank God for giving me this opportunity to learn and grow while in this graduate program. I am grateful for the support and love given by my mother Becky Dewitt, my father Anthony Cruickshank, my sister Ayesha Cruickshank, and other members of my family during my graduate studies; especially my Aunt Marva Vaught. Even though she could not live to see the end of this journey, she was critical to my success. I would to thank my childhood friends Jack Shamah and Marcus Smith for keeping me in line and always adding perspective.

My degree would not have been possible without many people at Clemson University. I would like to acknowledge my advisors (Dr. O. T. Mefford and Dr. M. Kennedy) and committee (Dr. E. Skaar) for their help. Dr. Kennedy and Dr. Mefford were patient during my learning process and inspired me to set high standards. I am very thankful for my committee member Dr. Skaar for talking me through technical issues and providing encouragement. Other faculty members, including Dr. J. DesJardins and Dr. M. Deqaq, allowed me to utilize equipment within their laboratories to complete these experimental plans. I am also very appreciative of the guidance provide by many of the faculty in the Materials Science and Engineering Department. In addition to faculty, I was supported by the members within my research groups who helped train me on structural and chemical characterization techniques including Dr. S. Saville, Dr. R. Stone and Dr. B. Qi, Ms. K. Davis and Mr. B. Fellows. Other students, Mr. D. Economy and Mr. B Schultz, helped train me on mechanical characterization and to accelerate my technical writing through new software and feedback.

TABLE OF CONTENTS

	Page
TITLE PAGE	i
ABSTRACT.....	ii
ACKNOWLEDGMENTS	iii
LIST OF TABLES	vii
LIST OF FIGURES.....	viii
CHAPTERS	
1. Introduction to Magnetic Nanoparticle Polymer Composite Membranes	1
1.1 Research Intent.....	1
1.2 Overview of Positive Displacement Pumps and Micropump Design	2
1.3 Magnetic Nanoparticles.....	5
1.3.1 Types of Magnetic Nanoparticles and Applications	7
1.3.2 Overview of Iron Oxide Nanoparticle Synthesis Via Co-Precipitation and Thermal Decomposition Methods	8
1.4 Introduction to MNPC Membranes and Applications	10
1.5 References	11
2. Magnetic Nanoparticle Membranes and Magnetic Deflection Determination	16
2.1 Introduction to Synthesis Methods for Constructing MNPC Systems	17
2.1.1 The Effect of MNPC Synthesis Method on the Mechanical Properties of the Membrane Systems	17
2.1.2 The Effect of MNPC Synthesis Method on the Structural Properties of the Membrane Systems	20

Table of Contents (Continued)

	Page
2.2 Mechanical and Magneto-Mechanical Testing of Membrane Systems.....	20
2.2.1 Introduction to Mechanical Testing of Membrane Systems via Pressure Deflection.....	22
2.2.2 Introduction to Magneto-Mechanical Analysis and Approximation of Volume Displaced.....	24
2.2.3 Clemson University Bulge Testing Apparatus and Augmentations for Magnetic Deflection	28
2.3 Summary	29
2.4 References.....	30
3. Materials for Constructing MNPC Membranes	
Characterization Methods	32
3.1 Nanoparticle Synthesis.....	32
3.2 MNPC and Metallic Film Processing	34
3.3 Sample Preparation for Characterization.....	36
3.4 Mechanical and Magneto-Mechanical Characterization	39
3.5 References	41
4. Results, Discussion, and Conclusion	42
4.1 Determining Method to Synthesizing Easy to Model Nanoparticles.....	42
4.2 Determining Method for MNPC Membrane Processing.....	45
4.3 Analysis and Comparison of Particle Clustering in MNPC Film Systems Processing.....	46
4.4 Analysis of the Metallica Layer System	47
4.5 Thickness Analysis of Film Systems	49
4.6 Preliminary Mechanical Characterization results of MNPC Membrane via Nano-DMA™	49
4.7 Results of Pressure Deflection Testing of MNPC Membranes	51
4.8 Results of Magnetic Deflection Testing of MNPC membranes.....	52
4.9 Results of Processing MNPC films with Higher Particle Concentrations	57

Table of Contents (Continued)

	Page
4.9.1 Analysis of Uncrosslinked MNPC Systems	58
4.10 Conclusions.....	60
4.11 References.....	62
5. Future Research Directions to Enhance Results	63
5.1 Possible Methods to Improve Current MNPC Structure through Fabrication	63
5.2 Enhancing the Magneto-Mechanical Characterization Capabilities	66
5.3 References.....	69
APPENDIX	70
A: Bulge Testing Operation	71

LIST OF TABLES

Table		Page
1.1	Table of different designs of micropumps systems using various actuation mechanisms and diaphragm materials	5

LIST OF FIGURES

Figure	Page
1.1 Representation of the three main categories of pumps	3
1.2 Representation of a diaphragm pump where A. is the driving force mechanism, B. membrane/diaphragm, C. chamber, and D. are the inlet and outlet check valves	4
1.3 Figure depicts how the moments, which are symbolized as the arrows within the particles, in superparamagnetic nanoparticles behavior changes from random to aligned when a magnetic field is applied.....	7
2.1 a.) Figure represents the composite b.) is a diagram representing the material from F. Fahrni et al	19
2.2 This a representative graph of the pressure deflection data when no slip or wrinkles are present during sample preparation.	23
2.3 This Caption is the side view of a deflected circular membrane that is bound at the edges. There variables in the this image coincide with determining the displacement volume during membrane deflection.....	27
2.4 Clemson University Bulge testing system with data flow schematic. Pressure values and rates are entered into the LabVIEW software, which then communicates to the pressure controller through the data acquisition component (DAQ). Pressure load is then applied to the testing stage, and both the laser vibrometer signal and the pressure signal from the transducer is relayed back to the software through the DAQ	28

List of Figures (Continued)

Figure	Page
3.1 This depiction shows how the layers of the film system will result after the MNPC construction process is completed. It should be noted that only the gold and the MNPC layers will be used for bulge testing and magnetic deflection	36
3.2 This is a relative depiction of were samples were harvested for testing. The blue boxes are the primary site for TOPO and Pneumatic and magnetic deflection. The green and red boxes are secondary and tertiary sites for magnetic and pneumatic deflection. The orange is the SEM site. The black and blue are the OM sites (i.e. clustering and surface changes). The black site is also for Nano-DMA™. The black dots represent the general scan area for TOPO measurements. All other squares are extra samples.....	38
4.1 TEM image of IONP synthesized by Hyeon et al. method, which displays particles of varying Geometries	42
4.2 TEM image of IONP synthesized using Sandia National Laboratory (unpublished research). (a.) Shows shape and size uniformity amongst the particles. (b.) shows the nanoparticle distribution	43
4.3 (a) Representative TEM image of sized and shape controlled particles. (b) The subsequent nanoparticle size analysis histogram.	44
4.4 MNPC film on a petri dish after the curing process	45
4.5 Image of a MNPC membrane on top of a mirrored steel substrate. The substrate allows for higher temperatures during the MNPC crosslinking process without deformation.....	46

List of Figures (Continued)

Figure		Page
4.6	Side-by side microscopy images of the the 5 wt. % (left) and (right) 0 wt. % samples	47
4.7	Metallic film that failed as a result of sample preparations.....	48
4.8	Example of a film sample with minimal damage during After sample preparations.....	49
4.9	Nano-DMA™ data of the 5 wt. % and 0 wt. % samples	50
4.10	Representative bulge test data with proper curvefit line without knowing Young’s Modulus values	52
4.11	Graph showing how the magnetic field of a ring magnet changes of distance	54
4.12	Depiction of the magnetic field of an axially magnetized ring magnet	54
4.13	Depiction of how a ring magnet is theorized to effects the MNPC membranes when the magnetic field gradient is greater in the lateral direction compared to the normal	56
4.14	Image of a MNPC system that failed to crosslink	57
4.15	FTIR analysis comparison between the extract of the failed MNPC sample, iron oleate, and oleic acid	59
A.1	Laser vibrometer computer and pressure controls	71
A.2	The components of the bulge testing stage where the deflection measurements are taken.	72

List of Figures (Continued)

Figure		Page
A.3	This is a representative graph of how slip appears in the data collected from bulge testing. The sample used for this representation went through two pressure cycles of ± 1 PSI Representative graph of sample slip appearing during bulge testing	74
A.4	Labview program front panel.....	76
A.5	DiaDiem software home screen	77

CHAPTER ONE

INTRODUCTION TO MAGNETIC NANOPARTICLE POLYMER COMPOSITE MEMBRANES

1.1 Research Intent

Magnetic nanoparticle polymer composites (MNPC) are polymeric materials designed to actuate in the presence of magnetic fields. A broad array of applications has been proposed in which these MNPCs could be used including cancer therapy, antimicrobial water treatment, microfluidic transport systems, and vibration/shock adsorption [1.1-1.5]. An additional application is the fabrication of MNPC membrane actuators for their inclusion in diaphragm pump devices. These devices could be remotely driven using a magnetic force (that is, the pump would not be connected physically to the actuating mechanism, but rather driven by an externally applied magnetic field [1.6, 1.7]).

Researchers have demonstrated that MNPC membrane deflection depends on the magnetic field, nanoparticle composition (magnetic properties of the nanoparticles), the membrane's concentration of those particles, and the stiffness of the membrane [1.5, 1.7, 1.8]. However, there are no reports that empirically relate MNPC membrane deflection to the applied magnetic field gradient [1.3, 1.8]. There is also a need to determine if the response of these membranes to mechanical or magnetic force are similar [1.9].

The objective of this thesis is to present a prototype MNPC membrane, and define the relationship between a MNPC membrane's structure and deflection during the application of external forces (magnetic and mechanical). We hypothesize that the membrane's behavior could be estimated by equating the mechanical force normally applied within

the generalized membrane mechanical deflection theorem [1.10, 1.11] with a simple Maxwell approximation of magnetic force [1.12, 1.13]. This thesis gives an overview of membrane pump development and design (Chapter 1), synthesis methods for magnetic nanoparticles used in MNPC systems (Chapter 2), fabrication and characterization methods used in this work (Chapter 3), structure property results for iron oxide nanoparticles (IONP's)-polydimethylsiloxane (PDMS) membranes in (Chapter 4), and future work needed to improve these preliminary results (Chapter 5).

1.2 Overview of Positive Displacement Pumps and Micropump Design

Pumps are apparatuses that transport fluid through mechanical action from one point in space to another [1.14]. While pumps originated around 300-200 BCE [1.15], there are still innovative designs being discovered. Though information about pump classification varies in literature; gravity, direct lift, and positive displacement are generally referenced as the three main categories [1.16], and examples are shown Figure 1.1. Gravity pumps uses the force of gravity to transport fluid [1.16]. Direct lift pumps use mechanical force to lift fluid from one reservoir to another fluid storage [1.16]. Positive displacement pumps apply mechanical force to a volume of fluid pushing it into a desired direction [1.16].

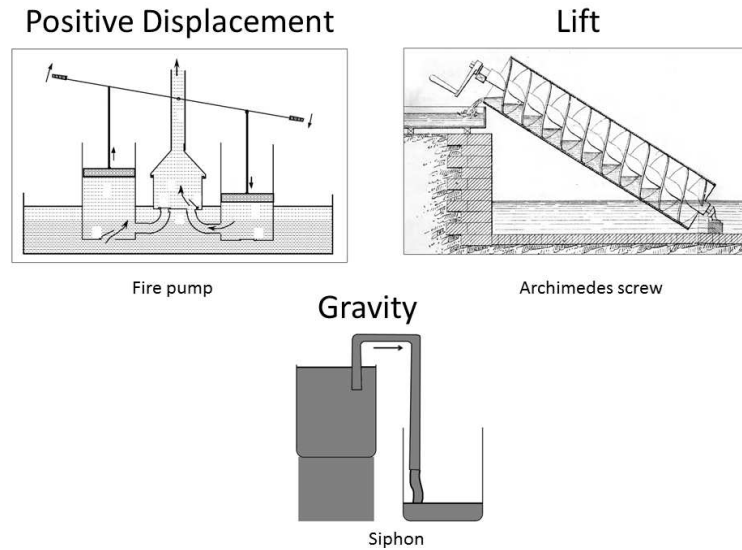


Figure 1.1: These images are representations of the main categories pumps. The images of the fire pump and the Archimedes screw were taken from Water Engineering of Ancient Civilizations [1.15]

Over the last 2000 years, variations of positive displacement pump systems have been developed due to both new applications being identified and design efficiency improvements [1.17]. One design category of these types of pump systems is the diaphragm pump [1.18], an example of which is shown in Figure 1.2. This system operates using a driver, diaphragm, chamber, and valve components [1.19]. The driver applies a force on the diaphragm, which then deflects and changes the internal volume of the chamber [1.19, 1.20]. The valves are used to direct the flow of fluid into and out of the chamber [1.19, 1.20].

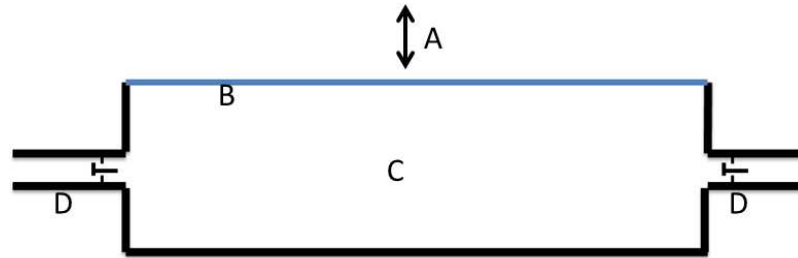


Figure 1.2 Representation of a diaphragm pump where A. is the driving force mechanism, B. the membrane/diaphragm, C. the chamber, and D. are the inlet and outlet check valves

A variant of the diaphragm pump is currently used for drug delivery [1.17, 1.20] to combat situation of patient harm due to medication related errors [1.21]. These medication related errors, such as inaccurate regulation of intravenous treatment, can result in adverse effects to patient harm [1.21] and it is estimated that 35% of all errors are related to the use of current medical pump systems [1.21]. New miniaturized pumps are being investigated to to deliver medication at low desired dosages, avoid contamination, and be driven with a small power source [1.22]. The design criteria for the use of these systems are high biocompatibility, drug compatibility, flow rate accuracy and precision, mostly-completely implantable, and small power consumption [1.17, 1.23, 1.24]. Research groups are investigating a range of actuation methods including piezoelectric, thermopneumatic, electrostatic, or electromagnetic drivers. A range of micropump systems that use different types of drivers can be seen in Table 1.1.

Electromagnetic drivers can supply a force remotely (i.e. distance between device and driver) and the applied magnetic fields can penetrate biological systems with minimal effect [1.17]. The electromagnetic pump designs generally fall into two types: systems where a permanent magnetic is attached at the center of the membrane [1.17, 1.24, 1.33],

or systems where the membrane is embedded with magnetic particles [1.3, 1.31, 1.39] that are micrometers or nanometers in size [1.7, 1.40-1.42]. The following section will discuss the properties of these particles embedded in MNPC.

Table 1.1: Table of authors that designed micropump systems using various actuating mechanisms and diaphragm materials

Driver	Diaphragm material	Membrane dimensions	Deflection/flow rate measurement system
Piezoelectric	Si	4 mm x 8 mm x 70 μm	Laser interferometry [1.26]
Piezoelectric	PDMS	Thickness 100-200 μm	Micro-PIV [1.27]
Electrostatic	Si	1.7 mm x 1 mm x 15 μm	Not recorded [1.28]
Electrostatic	Si	1.7 mm x 1 mm x 15 μm	Not recorded [1.29]
Thermopneumatic	Si	7 mm x 7 mm x 10-30 μm	Syringe pump [1.30]
Electromagnetic	PDMS	Not recorded	Laser interferometry [1.31]
Electromagnetic	PDMS	4-7mm diameter 34-37 μm thickness	Optical microcopy [1.32]
Electromagnetic	PDMS	10 mm diameter 0.1- 0.5 mm thickness	Laser interferometry [1.33]
Bimetallic	Al-Si	Not recorded	Not recorded [1.34]
Electrowetting	Silicone	5.6 mm x 5.6 mm x 80 μm	Laser interferometry [1.35]
Shape memory alloy	Ti, Ni	8.4 mm x 8.4 mm x 10 μm	Not recorded [1.36]
Shape memory alloy	Ti, Ni, Si	3.7 mm x 3.7mm x 7 μm	Laser interferometry [1.37]
Phase change	Si	30 μm Thickness	Laser interferometry [1.38]

1.3 Magnetic Nanoparticles

Nanoparticle dimensions (diameter) are known to affect the domain (regions of uniform magnetic moments with the material separated by domain walls [1.43]) and superparamagnetic limits (the ability to easily flip the magnetization of the magnetic material due to thermal energy fluctuations [1.43]). Below a critical diameter for spherical particles, the particles are considered to have a single domain and exhibit a uniform magnetic moment [1.43, 1.44]. The critical diameter, D_c , of the magnetic domain has been previously expressed as:

$$D_c \approx 18 \frac{\sqrt{AK_{eff}}}{\mu_0 M^2} \quad (1.1)$$

where A is the exchange constant (i.e. the measure of interaction strength between adjacent electron spins due to the exchange interaction [1.45]), K_{eff} is the effective anisotropy constant, μ_0 is the permeability of free space, M is the saturation magnetization of the particle.

The energy responsible for pinning the magnetic moment in a particular direction is the magnetic anisotropy energy $E(\theta)$ [1.43, 1.44, 1.46, 1.47], and is expressed as:

$$E(\theta) = K_{eff}V \sin^2 \theta \quad (1.2)$$

where V is the particle volume and θ is the angle between the magnetization and the energetically favorable direction of which magnetic moments align. When the size of the magnetic nanoparticle is reduced below this threshold value, the magnetic anisotropy energy is comparable with the thermal activation energy, $k_B T$, where k_B is Boltzmann's constant [1.47]. By reducing the particle diameter, the energy associated with pinning the magnetic moment in a particular direction is depressed [1.43, 1.47]. This allows the moment of the particle to be randomly orientated above a certain temperature, until a magnetic field is applied to the system as depicted in Figure 1.3 [1.48].

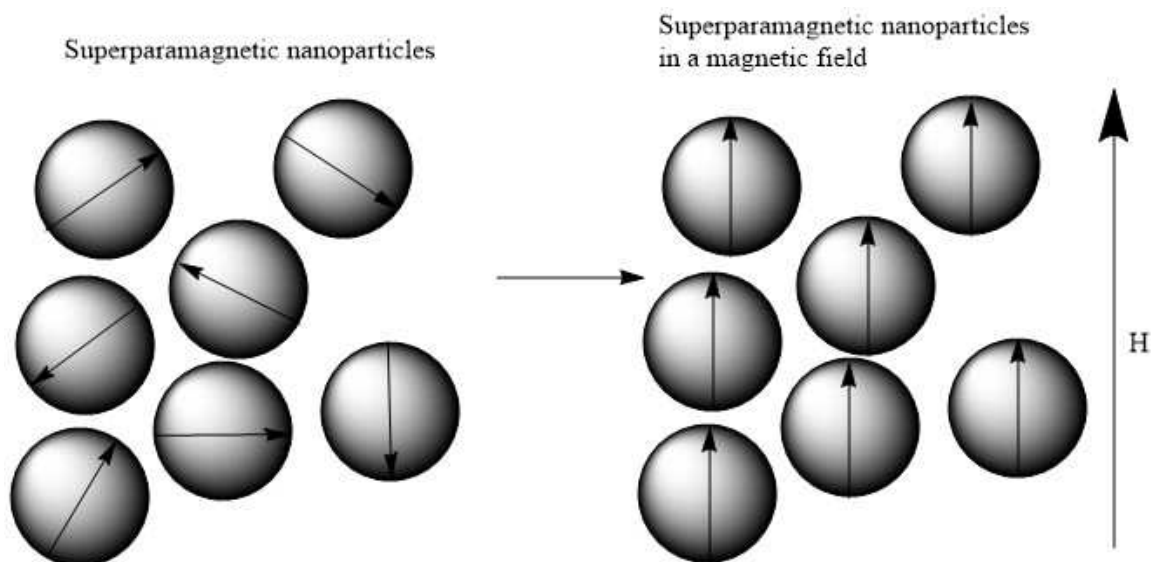


Figure 1.3 Figure depicts how the moments, which are symbolized as the arrows, in superparamagnetic nanoparticles behavior changes from random to aligned when a magnetic field is applied.

1.3.1 Types of Magnetic Nanoparticles and Applications

Nanoparticles used for biomedical applications are primarily iron oxide based nanoparticles (IONPs) [1.49], but other compositions have been investigated for nano-based biomedical research [1.50-1.52]. For example, doped gadolinium oxide nanoparticles were used by Zhou et al. to serve as a bioimaging and magnetic resonance imaging contrast agent [1.53]. These researchers were able to develop a method for creating size controlled Gd_2O_3 nanoparticles and then doping those particles with other lanthanide series ions. It was observed that this material fluoresces under near infrared excitation and can be seen in a dark room. Cobalt have been studied in applications such as membranes for micro pumps [1.54] and bio actuation applications [1.40]. Like pure iron, pure cobalt has high magnetization saturation, which determines the amount of magnetic field necessary to move the material [1.40]. Unfortunately, pure cobalt readily

oxidizes unless coated with an inorganic species [1.40, 1.52], and the oxidized species of cobalt is toxic to the human body [1.52, 1.55]. Generally, the synthesis of forming these particles is very similar to each other, in that the particles are formed via chemical or physical alterations from a starting material.

1.3.2 Overview of Iron Oxide Nanoparticle Synthesis Via Co-Precipitation and Thermal Decomposition Methods

IONPs are generally synthesized through either a physical or chemical method [1.56, 1.57]. Physical methods such as ball-milling break bulk materials down to a desired size distribution [1.56, 1.57]. Though the concept of the physical process is straightforward, the processing time for grinding particles of a consistent size can take days [1.57]. It also produces particles of varying shapes with large size distributions [1.56, 1.57].

Chemical methods such as co-precipitation or thermal decomposition alter reaction species to synthetically grow nanoparticles [1.58]. The chemical approach for synthesizing nanoparticles has demonstrated the capability to consistently produce particles with a uniform shape and small size dispersion in less time than the physical process [1.59]. To have a uniform set of properties, nanoparticles are generally synthesized via chemical method, especially for bio-applications [1.59].

The co-precipitation method is the most common and simplest route for synthesizing IONPs [1.58]. By increasing the pH (8-14) of an aqueous solution of

ferrous and ferric salt in an inert atmosphere, magnetite (Fe_3O_4) nanoparticles will precipitate [1.43, 1.58]. The expected reaction will be:



The main advantage to this method is its ability to synthesize large amounts of nanoparticle in a batch in less time than the physical approach [1.57, 1.58]. Unfortunately, this method is limited in its ability to restrict the particle size distribution due do to kinetic factors that primarily controls the particle growth [1.43, 1.58].

Another common chemical method, thermal decomposition, makes up for the coprecipitation method's lack of particle size control during the nanofabrication process [1.43]. In this process, nanoparticles are produced by thermally decomposing an organometallic compound in a high boiling point organic solvent containing a stabilizing surfactant [1.43]. Generally, the organometallic precursors used in this reaction are metal acetylacetonate ($M(C_5H_7O_2)_n$), metal cupferronate ($M(C_6H_5N_2O_2)_n$), or metal carbonyl ($M(CO)_n$) [1.43]. By controlling the ratios of the starting reagents, reaction temperature, and reaction time, precise control over size and nanoparticle morphology will be attained. Though this method produces nanoparticles with a small size distribution, the particles are hydrophobic due to the surfactant that covers the surface of the particles [1.43] and need to be modified prior to use in biological settings. Overall, both methods have their advantages and have been observed in MNPC materials [1.41, 1.54, 1.60].

1.4 Introduction to MNPC Membranes and Applications

There have been many instances of magnetic particles in a polymeric matrix within small-scale devices [1.31, 1.32, 1.61, 1.62]. These systems have been effectively demonstrated in a range of application spanning from valve-less micropumps and miniature reservoirs to filtration systems [1.32, 1.63, 1.64, 1.66-1.68]. These composite materials have the advantages of low cost of processing and low elastic modulus [1.8]. For diaphragm micropumps, low elastic moduli equates to large attainable deflection within the system [1.69]. This is important since deflection is proportional to the volume of fluid displaced [1.69]. In 2004, Yamahata et al. demonstrated relatively large deflections using a microfluidic device [1.65]. This utilized a thermosetting PDMS circular membrane able to deflect up to 200 μm . Another micropump system design (micro-reservoir) was fabricated by Pirmoradi et al. in 2011 [1.32]. This system used a porous PDMS magnetic composite membrane as the actuating component, with a diameter of 6 mm and thickness of 40 μm . The largest measured deflection attained by this membrane system was 219 μm . Other applications for MNPC include filtration systems [1.66-1.68]. Dudek et al. explored the effect of embedding magnetic nanoparticles in gas permeable polymer membranes [1.67]. In this study, poly 2,6-dimethyl-1,4-phenylene oxide 25 μm thick membranes were impregnated with iron oxide particles with the intent of establishing a gas selective system. This was observed by attempting to permeate gas mixtures of oxygen and nitrogen through the MNPC membrane system, which was effectively separated due to the paramagnetic properties of oxygen. This control over gas diffusion through MNPC membrane materials was also

observed in Rybak et al. [1.68]. Overall these systems have successfully been used in array of applications.

1.5 References

- [1.1] Sarkar, Guibal, Quignard, Sengupta, Polymer-Supported Metals and Metal Oxide Nanoparticles: Synthesis, Characterization, and Applications, *Journal of Nanoparticle Research*, 14, (2012) 1-24
- [1.2] Gray, A Review of Magnetic Composite Polymers Applied to Microfluidic Devices, *Journal of the Electrochemical Society*, 161, (2014) B3173-B3183.
- [1.3] Wang, Yao, Chen, Fang, Composite Elastic Magnet Films with Hard Magnetic Feature, *Journal of Micromechanics and Microengineering*, 14, (2004) 1321-1327.
- [1.4] Li, Zhang, Wang, Li, Sheng, Wen, Design and Fabrication of Microfluidic Mixer from Carbonyl Iron–PDMS Composite Membrane, *Microfluidics and Nanofluidics*, 10, (2010) 919-925.
- [1.5] Snyder, Nguyen, Ramanujan, Design Parameters for Magneto-Elastic Soft Actuators, *Smart Materials and Structures*, 19, (2010) 055017.
- [1.6] Suter, Ergeneman, Schmid, Camenzind, Nelson, Hierold, Superparamagnetic Photosensitive Polymer Nanocomposite for Microactuators, *IEEE*, (2009) 869-872.
- [1.7] Fahrni, Prins, Van Ijzendoorn, Magnetization and Actuation of Polymeric Microstructures with Magnetic Nanoparticles for Application in Microfluidics, *Journal of Magnetism and Magnetic Materials*, 321, (2009) 1843-1850.
- [1.8] Pirmoradi, Cheng, Chiao, A Magnetic Poly(Dimethylesiloxane) Composite Membrane Incorporated with Uniformly Dispersed, Coated Iron Oxide Nanoparticles, *Journal of Micromechanics and Microengineering*, 20, (2010) 015032.
- [1.9] Thangawng, Ruoff, Swartz, Glucksberg, An Ultra-Thin PDMS Membrane as a Bio/Micro–Nano Interface: Fabrication and Characterization, *Biomedical Microdevices*, 9, (2007) 587-595.
- [1.10] Vlassak, New Experimental Techniques and Analysis Methods for the Study of the Mechanical Properties of Materials in Small Volumes, *Stanford University*, (1994).
- [1.11] Vinci, Mechanical Behavior of Thin Films, *Annual Reviews Materials Science*, 26, (1996) 33.
- [1.12] Mefford, Woodward, Goff, Vadala, St. Pierre, Dailey, Riffle, Field-Induced Motion of Ferrofluids through Immiscible Viscous Media: Testbed for Restorative Treatment of Retinal Detachment, *Journal of Magnetism and Magnetic Materials*, 311, (2007) 347-353.
- [1.13] Pankhurst, Connolly, Jones, Dobson, Applications of Magnetic Nanoparticles in Biomedicine *Journal of Physics D: Applied Physics*, 36, (2003) 15.
- [1.14] Bloch, *Pump User's Handbook: Life Extension*, (2006) 488.
- [1.15] Pierre-Louis, *Water Engineering in Ancient Civilizations 5,000 Years of History*, (2005) 322.
- [1.16] Fraenkel, Chapter 3: Review of Pumps and Water Lifting Techniques, in: *Water Lifting Devices*, Food and Agriculture Organization of the United Nations, Rome, Italy, (1986), 35-49.
- [1.17] Nisar, Afzulpurkar, Mahaisavariya, Tuantranont, MemS-Based Micropumps in Drug Delivery and Biomedical Applications, *Sensors and Actuators B: Chemical*, 130, (2008) 917-942.

- [1.18] Nisbitt, Handbook of Pumps and Pumping, (2006) 470.
- [1.19] Pump Characteristics and Applications, Second Edition, Taylor & Francis Group, (2005).
- [1.20] Krassimir, Trencheva, Micropumps ofr Medical Applications, Electronic, Sozopol, Bulgaria, (2007), 165-170.
- [1.21] Breland, Continuous Quality Improvement Using Intelligent Infusion Pump Data Analysis., American journal of health-system pharmacy : AJHP : Official Journal of the American Society of Health-System Pharmacists, 67, (2010) 1446-1455.
- [1.22] Cao, Mantell, Polla, Design and Simulation of an Implantable Medical Drug Delivery System Using Microelectromechanical Systems Technology, Sensors and Actuators A: Physical, 94, (2001) 117-125.
- [1.23] Grayson, Shawgo, Johnson, Flynn, Li, Cima, Langer, A Biomems Review: Mems Technology for Physiologically Integrated Devices, Proceedings of the IEEE, 92, (2004) 6-21.
- [1.24] Woias, Micropumps – Summarizing the First Two Decades, 4560 (2001) 39-52.
- [1.25] Laser, Santiago, A Review of Micropumps, Journal of Micromechanics and Microengineering, 14, (2004) R35-R64.
- [1.26] Koch, Harris, Evans, White, Brunnschweiler, A Novel Micromachined Pump Based on Thick-Film Piezoelectric Actuation, Sensors and Actuators A: Physical, 70, (1998) 98-103.
- [1.27] Suzuki, Teramura, Hata, Inokuma, Kanno, Hiroo, Hidetoshi, Development of a Micro Biochip Integrated Traveling Wave Micropumps and Surface Plasmon Resonance Imaging Sensors ASME/JSME Joint Conference on Micromechatronics for Information and Precision Equipment, Santa Clara, CA, (2006).
- [1.28] Zengerle, A Didirectional Silicon Micropump, Sensors and Actuators A: Physical, 50, (1995) 81-86.
- [1.29] Richter, Linnemann, Woias, Robust Design of Gas and Liquid Micropumps, Sensors and Actuators A: Physical, 68, (1998) 480-486.
- [1.30] Elwenspoek, Lammerink, Miyakei, Towards Integrated Microliquid Handling Systems, 4, (1994) 227-245.
- [1.31] Lederer, Heinisch, Hilber, Jakoby, Electromagnetic Membrane-Pump with an Integrated Magnetic Yoke, IEEE Sensors, (2009) 532-537.
- [1.32] Pirmoradi, Jackson, Burt, Chiao, A Magnetically Controlled Mems Device for Drug Delivery: Design, Fabrication, and Testing, Lab on a Chip, 11, (2011) 3072.
- [1.33] Hilber, Jakoby, A Magnetic Membrane Actuator Utilizing Diamagnetic Levitation, IEEE Sensors, (2012) 1-4.
- [1.34] Zou, Ye, Zhou, Yang, A Novel Thermally Actuated Micropump, Proceedings of the 1997 International Symposium on Micromechatronics and Human Science, (1997), 231-234.
- [1.35] Yun, Cho, Bu, Kim, Yoon, A Surface-Tension Driven Micropump for Low-Voltage and Low-Power Operations, Journal of Microelectromechanical Systems, (2002) 454-461.
- [1.36] Benard, Kahn, Heuer, Huff, Thin-film Shape Memory Alloy Actuated Micropumps, Journal of Miroelectromechanical Systems, 7, (1998) 245-251.

- [1.37] Xu, Wang, Ding, Zhou, Yu, Cai, Characteristics and Fabrication of Niti/Si Diaphragm Micropump, *Sensors and Actuators A: Physical*, 93, (2001) 87-92.
- [1.38] Sim, Yoon, Jeong, Yang, A Phase-Change Type Micropump with Aluminum Flap Valves, *Journal of Micromechanics and Microengineering* 13 (2003) 286-294.
- [1.39] Wang, Polydimethylsiloxane Mechanical Properties Measured by Macroscopic Compression and Nanoindentation Technique, University of South Florida, (2011).
- [1.40] Fuhrer, Athanassiou, Luechinger, Stark, Crosslinking Metal Nanoparticles into the Polymer Backbone of Hydrogels Enables Preparation of Soft, Magnetic Field-Driven Actuators with Muscle-Like Flexibility, *Small*, 5, (2009) 383-388.
- [1.41] Evans, Fiser, Prins, Rapp, Shields, Glass, Superfine, A Highly Tunable Silicone-Based Magnetic Elastomer with Nanoscale Homogeneity, *Journal of Magnetism and Magnetic Materials*, 324, (2012) 501-507.
- [1.42] Nanni, Petroni, Fragouli, Amato, De Vittorio, Athanassiou, Microfabrication of Magnetically Actuated PDMS–Iron Composite Membranes, *Microelectronic Engineering*, 98, (2012) 607-609.
- [1.43] Lu, Salabas, Schüth, *Magnetic Nanoparticles: Synthesis, Protection, Functionalization, and Application*, *Angewandte Chemie International Edition*, 46, (2007) 1222-1244.
- [1.44] Bean, Livingston, Superparamagnetism, *Journal of Applied Physics*, 30, (1959) S120.
- [1.45] Vaz, Bland, Lauhoff, Magnetism in Ultrathin Film Structures, *Reports on Progress in Physics*, 71, (2008) 1-79.
- [1.46] Laurent, Dutz, Häfeli, Mahmoudi, Magnetic Fluid Hyperthermia: Focus on Superparamagnetic Iron Oxide Nanoparticles., *Advances in Colloid and Interface Science*, 166, (2011) 8-23.
- [1.47] Rondinone, Samia, Zhang, Superparamagnetic Relaxation and Magnetic Anisotropy Energy Distribution in CoFe₂O₄ Spinel Ferrite Nanocrystallites, *The Journal of Physical Chemistry B*, 103, (1999) 6876-6880.
- [1.48] Douglass, Cox, Bucher, Bloomfield, Magnetic Properties of Free Cobalt and Gadolinium Clusters, *Physical Review B*, 47, (1993) 12874-12889.
- [1.49] Gupta, Gupta, Synthesis and Surface Engineering of Iron Oxide Nanoparticles for Biomedical Applications, *Biomaterials*, 26, (2005) 3995-4021.
- [1.50] Zhou, Size-Tunable Synthesis of Lanthanide-Doped Gd₂O₃ Nanoparticles and Their Applications for Optical and Magnetic Resonance Imaging, *Journal of Materials Chemistry*, 22, (2012) 966-974.
- [1.51] Xiao, Li, Nanocomposites: From Fabrications to Electrochemical Bioapplications, *Electroanalysis*, 20, (2008) 648-662.
- [1.52] Bao, Krishnan, Preparation of Functionalized and Gold-Coated Cobalt Nanocrystals for Biomedical Applications, *Journal of Magnetism and Magnetic Materials*, 293, (2005) 15-19.
- [1.53] Zhou, Gu, Liu, Yin, Tian, Yan, Jin, Ren, Xing, Li, Chang, Hu, Zhao, Size-Tunable Synthesis of Lanthanide-Doped Gd₂O₃ Nanoparticles and Their Applications for Optical and Magnetic Resonance Imaging, *Journal of Materials Chemistry*, 22, (2012) 966.

- [1.54] Singh, Shirolkar, Limaye, Gokhale, Khan-Malek, Kulkarni, A Magnetic Nano-Composite Soft Polymeric Membrane, *Microsystem Technologies*, 19, (2012) 409-418.
- [1.55] Rhoads, Lung Clearance, Translocation, and Acute Toxicity of Arsenic, Beryllium, Cadmium, Cobalt, Lead, Selenium, Vanadium, and Ytterbium Oxides Following Deposition in Rat Lung, *environmental research*, 36, (1985) 21.
- [1.56] Chakka, Altuncevahir, Jin, Li, Liu, Magnetic Nanoparticles Produced by Surfactant-Assisted Ball Milling, *Journal of Applied Physics*, 99, (2006) 08E912.
- [1.57] Can, Ozcan, Ceylan, Firat, Effect of Milling Time on the Synthesis of Magnetite Nanoparticles by Wet Milling, *Materials Science and Engineering: B*, 172, (2010) 72-75.
- [1.58] Laurent, Dutz, Hafeli, Mahmoudi, Magnetic Iron Oxide Nanoparticles: Synthesis, Stabilization, Vectorization, Physicochemical Characterizations, and Biological Applications, *Chemical Reviews*, 108, (2008) 47.
- [1.59] Roca, Morales, O'grady, Serna, Structural and Magnetic Properties of Uniform Magnetite Nanoparticles Prepared by High Temperature Decomposition of Organic Precursors, *Nanotechnology*, 17, (2006) 2783-2788.
- [1.60] Sarkar, Guibal, Quignard, SenGupta, Polymer-Supported Metals and Metal Oxide Nanoparticles: Synthesis, Characterization, and Applications, *Journal of Nanoparticle Research* (2012) 1-24.
- [1.61] Ju, Ju, Saka, Liu, Wan, A Systematic Method for Characterizing the Elastic Properties and Adhesion of a Thin Polymer Membrane, *International Journal of Mechanical Sciences*, 47, (2005) 319-332.
- [1.62] Nie, Huang, Li, Measurement of Residual Stress in Multilayered Thin Films by a Full-Field Optical Method, *Sensors and Actuators A: Physical*, 126, (2006) 93-97.
- [1.63] Lee, Weng, Cheng, Yeh, Lei, Lee, Biomedical Microdevices Synthesis of Iron Oxide Nanoparticles Using a Microfluidic System, *Biomedical Microdevices*, 11, (2008) 161-171.
- [1.64] Loverich, Kanno, Kotera, Concepts for a New Class of All-Polymer Micropumps., *Lab-On-A-Chip*, 6, (2006) 1147-1154.
- [1.65] Yamahata, Lotto, Al-Assaf, Gijs, A PMMA Valveless Micropump Using Electromagnetic Actuation, *Microfluidics and Nanofluidics*, 1, (2004) 197-207.
- [1.66] Homayoonfal, Mehrnia, Mojtahedi, Ismail, Effect of Metal and Metal Oxide Nanoparticle Impregnation Route on Structure and Liquid Filtration Performance of Polymeric Nanocomposite Membranes: A Comprehensive Review, *Desalination and Water Treatment*, 51, (2013) 3295-3316.
- [1.67] Dudek, Turczyn, Strzelewicz, Rybak, Krasowska, Grzywna, Preparation and Characterization of Iron Oxides – Polymer Composite Membranes, *Separation Science and Technology*, 47, (2012) 1390-1394.
- [1.68] Rybak, Grzywna, Kaszuwara, On the Air Enrichment by Polymer Magnetic Membranes, *Journal of Membrane Science*, 336, (2009) 79-85.
- [1.69] Hall, Apperson, Crozier, Xu, Richards, Bahr, Richards, A Facility for Characterizing the Dynamic Mechanical Behavior of Thin Membranes for Microelectromechanical Systems, *Review of Scientific Instruments*, 73, (2002) 2067.

CHAPTER TWO

MAGNETIC NANOPARTICLE MEMBRANES AND MAGNETIC DEFLECTION DETERMINATION

The efficiency of micropumps and magnetic micropumps can be improved through both new designs and materials [2.1]. While the central deflection of membranes within membrane micropumps can be measured when a mechanical force or magnetic field gradient is applied, it would be preferable to predict these deflections as a function of the mechanical properties, magnetic properties, and membrane geometry [2.2-2.5]. The geometric properties of the MNPC membranes are the membrane thickness, diameter and the window geometry- all of which are used to predict deflection under pneumatic loading for homogeneous membranes [2.2-2.4].

The average core diameter of the nanoparticles has been used to determine the magnetic properties of the system. If it is assumed that the magnetic nanoparticles of the system are superparamagnetic, an estimate the magnetization of the nanoparticles in the composite system can be found by using a Langavim function to approximate the magnetization as a function of field [2.6, 2.8]. The magnetization of the nanoparticles is important in estimating the magnetic force applied to a MNPC system because it is a measure of the net dipole moments within the material that orientate towards the applied magnetic field [2.8].

In this chapter, a brief description of methodology for synthesizing MNPC membranes will be discussed (Section 2.1). This will include an analysis of the two major membrane synthetic methodologies and the observed effects of these techniques on

the membrane's mechanical properties, structural properties, and thus the attainable deflection of the membrane. Section 2.2 will be a discussion on membrane characterization via pressure deflection. This will include details on approximating magnetic deflection, volume displacement, and measurement error using a bulge test system.

2.1 Introduction to Synthesis Methods for Constructing MNPC Systems

Literature has shown that there are various methods for constructing MNPC systems [2.5-7, 2.13, 2.14], which can be put into two main categories, the *ex-situ* and *in-situ* methods [2.13, 2.14]. The *ex-situ* method uses pre-synthesized nanoparticles and polymer to form the composite material [2.13, 2.14]. Typically, the nanoparticles are encapsulated within a polymer matrix that has been crosslinked [2.5, 2.6, 2.9, 2.15]. The *in-situ* approach synthesizes nanoparticles within the preformed polymer matrix (mainly through a derivative version of the co-precipitation method), or crosslinking the ligands on the nanoparticles to form the composite matrix [2.13, 2.14, 2.16]. The synthesis method used to produce the composite membrane will affect the mechanical and structural properties of the system [2.5, 2.7].

2.1.1 The Effect of MNPC Synthesis Method on the Mechanical Properties of the Membrane System

The fabrication method has been shown to alter elastic modulus of a system keep the architecture and chemistry similar [2.5-2.7, 2.13]. It has been shown that the

magnetoelastic ratio (i.e. the weight/volume loading of particles in the material divided by the elastic modulus of the material) varies depending on the method of construction [2.5-2.7, 2.13, 2.14, 2.17]. For example, both Fahrni et al. and Evans et al. demonstrated the synthesis of MNPC systems using PDMS as the matrix and IONPs as the filler using two different methods of construction [2.6, 2.7]. Fahrni et al. used an *ex-situ* method by mixing magnetic nanoparticles that had surfactant on the surface with Sylgard 184 (PDMS) prepolymer prior to crosslinking. This was achieved by adding an IONP powder to tetrahydrofuran (THF) and then mixing it in the PDMS prepolymer. The THF was then evaporated before the curing agent was mixed with the system. They used this method to construct multiple samples with varying weight percentages and found that the elastic modulus of the system decreased as the weight percent of nanoparticles increased [2.6]. This trend is later seen in another publication, Pirmoradi et al., where this effect was cited as being caused by the poor adhesion between the surface of the nanoparticle and polymer matrix [2.5]. Evans et al. used the *in-situ* method by adding the nanoparticles and then crosslinking the PDMS ligand on the surface of the particles to form the matrix. This was achieved by using a co-precipitation process IONPs, and then forming a particle complex by binding a 3,000 g/mol aminopropylmethylsiloxane co-dimethylsiloxane (PDMS-NH₂) to the particle surface. The complex was then crosslinked by adding dicumyl peroxide and heating it to 180°C for 2 hours. This method was used to form composites with varying particle weight percentages, and for this MNPC process, it was seen that the modulus for the structure increased as particle concentration increased [2.7]. This was also seen in the publication of Song et al. where

the nanoparticles were used to crosslink the polymer matrix, increasing the elastic modulus of the composite as opposed to decreasing it [2.13]. These observations suggest that the mechanical properties of these composites are directly affected by how the nanoparticles are bound in the system. Thus, it is important to consider the method of construction for it will deduce the outcome of the mechanical properties of these systems. Figure 2.1 depicts a simplified diagram that represents resulting materials from both fabrication routes.

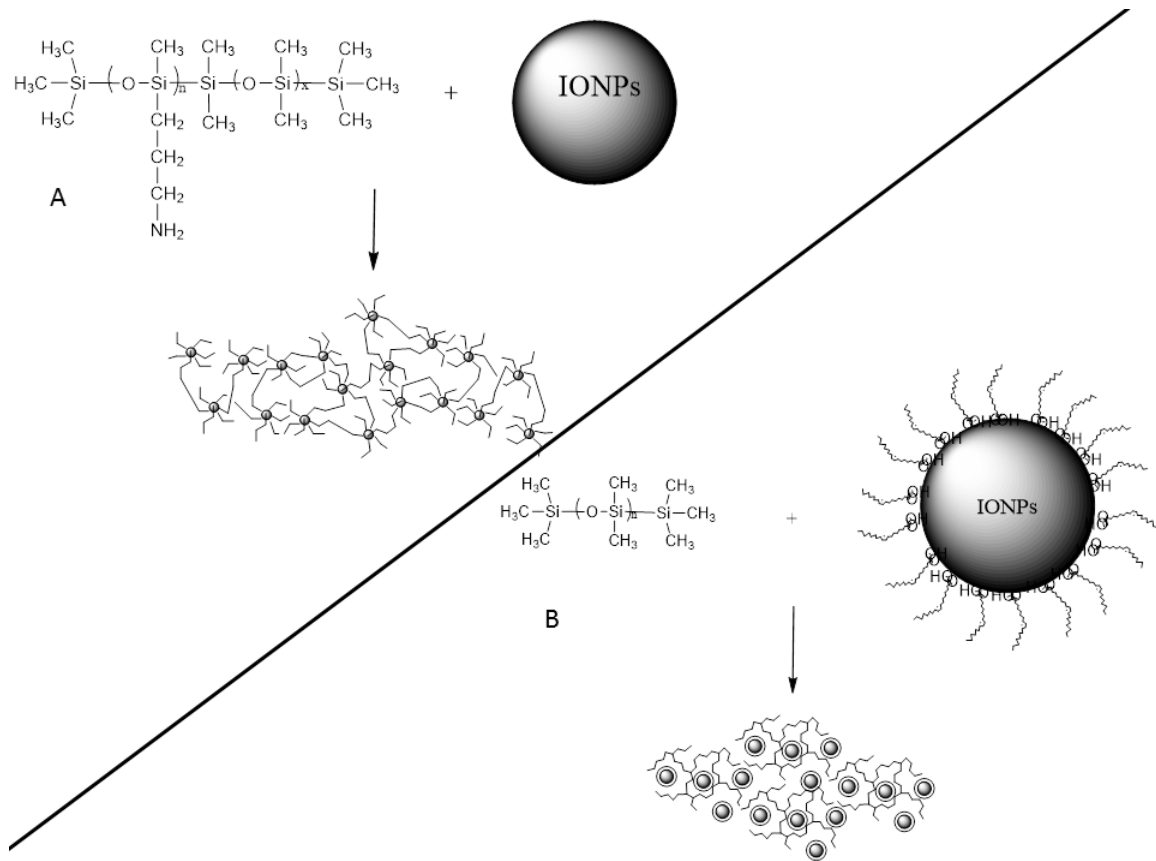


Figure 2.1: A.) is a diagram representing the composite material from B. Evans et al. B.) is a diagram representing the material from F. Fahrni et al.

2.1.2 The Effect of MNPC Synthesis Method on the Structural Properties of the Membrane System

The structural properties most affected by the synthesis method are the thickness and the nanoparticle agglomeration size [2.1, 2.7, 2.14]. Within MNPC membrane studies, many groups reference the formation of nanoparticle agglomerations [2.5, 2.6] which can impact the ability to distribute the nanoparticles throughout the membrane. The nanoparticle dispersion in the polymer matrix could be important, because it could alter the membrane response under magnetic stimuli [2.5, 2.7]. For example, large particles could apply a larger magnetic force within a gradient compared to smaller particles. Using the *ex-situ* method, the composite system tends to have large aggregates [2.5]. This becomes an issue when designing systems with dimensions that would be smaller than the largest particle agglomeration [2.5-2.7].

The core diameter of the nanoparticles can be also affected by the choice synthesis method [2.14, 2.18]. The *ex-situ* methods have not been shown to affect the final nanoparticle diameter, for the nanoparticles are synthesized prior to the composites construction [2.5, 2.6, 2.14, 2.19]. However, some *in-situ* methods have been observed to influence the final nanoparticle size and shape [2.14, 2.18].

2.2 Mechanical and Magneto-Mechanical Testing of Membrane Systems

Many groups have studied how polymeric membranes deform under pneumatic force, through both experimental validation and the creation of analytical models [2.5, 2.9]. The deflection at the center of a membrane due to an applied pneumatic force can

be experimentally determined through the use of a bulge testing system [2.2, 2.3, 2.4, 2.9]. This method characterizes the free standing thin film window (i.e. membrane) of a material by applying a known pressure to one side and measuring the deflection height [2.3, 2.4]. This technique is commonly performed on metals and ceramic materials, but has been used in the characterization of polymeric films [2.4, 2.10, 2.11]. This was demonstrated by Huang et al., where bulge testing was used in determining the mechanical properties of poly methyl methacrylate (PMMA) films with thicknesses ranging from 77 nm to 352 nm [2.11]. This study determined the Young's modulus of the PMMA films to be 5.2 GPa. The use of this technique on soft materials was demonstrated by Thangawng et al. [2.12]. In this study, the mechanical properties of 70 nm thick polydimethylsiloxane films were investigated for the purpose of being a bio interface for studying cellular mechanics.

An extension of these is needed to account for magnetic force in MNPC membrane applications with biopumps (i.e. a pump system that is implantable). Only a few articles have identified the relationship between pneumatic and magnetic forces on a membrane and the membrane's deflection [2.5, 2.9]. Wang et al. used micrometer sized particles within their membranes and observed the membrane deflection during the application of a magnetic field [2.9]. In this study, they assumed a nonlinear relationship between pneumatic and magnetic loading could evaluate the deflection attained during membrane stimulation. Pirmoradi et al. in 2010 observed a non-linear relationship between the pressure caused by the magnetic field and deflection [2.5]. Continuing

previous efforts, the following sections will try to predict magnetic deflection based on prior membrane pneumatic pressure - deflection relationships.

2.2.1 Introduction to Mechanical Testing of Membrane Systems via Pressure

Deflection

Bulge testing has been used to character the mechanical properties of thin film polymer and polymer composite systems [2.3, 2.17, 2.20-2.22]. The magnitude of deflection of membranes depends primarily on the geometry of the membrane window, the applied pressure, and the mechanical properties of the material [2.23]. Vlassak et al. and Vinci et al. developed the generalized bulge equation (equation 2.1) that describes the response of a pressurized thin film system [2.2, 2.4]. The applied pressure, P, is

$$P = \frac{c_1 \sigma_0 t / h}{a^2} + \frac{c_2 E t / h^3}{(1-\nu) a^4} \quad (2.1)$$

where a is the radius of a circular membrane, t is the thickness of the membrane, c₁ and c₂ are geometric constants that relate to the shape and Poisson's ratio membrane, σ₀ is the residual stress within the film, E is the elastic modulus, ν is Poisson's ratio of the sample, and h is the deflection height of the membrane center [2.3, 2.4, 2.17, 2.23]. The resulting data should be similar to the graph in Figure 2.2 when pressure is plotted against deflection.

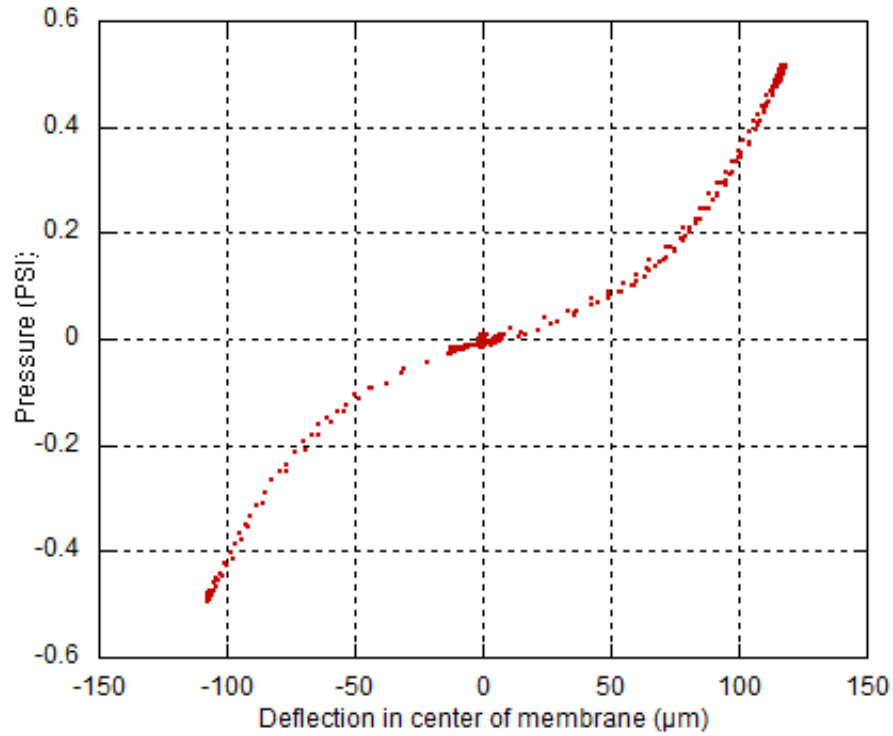


Figure 2.2: This a representative graph of the pressure deflection data when no slip or wrinkles are present during sample preparation.

Curve fitting this equation to the pressure/deflection data of a bulge test [2.3, 2.4, 2.25] allows for the determination of the elastic modulus or the residual stress in the film due to processing [2.2, 2.4, 2.24]. The fabrication method for each membrane will control the mechanical properties of the membrane. For example, the fabrication method has been shown to alter elastic modulus of the composite system

2.2.2 Response of Magnetic Particles of Magnetic Fields

When a magnetic field is applied to a MNPC membrane, the center membrane deflection is related to the force applied on the nanoparticles. This force on the system, F_m , can be described by:

$$F_m = \mu_0 \nabla (m \cdot H) \quad (2.2)$$

where μ_0 is the permeability of free space, m is the magnetic moment of the system, and H is the applied magnetic field [2.8]. The contributing variables that affect the magnetic force are the magnetization of the particles, the total volume of particles within the membrane, and the gradient of the applied magnetic field. If it is assumed that the magnetization of particles is along the direction of the magnetic field and that only the field gradients along that direction are considered [2.8], then Equation 2.2 can be reduced to

$$F_m = VM_{(x)} \frac{dH}{dx} \quad (2.3)$$

where V is the volume of magnetic particles, M is the magnetization of those particles in the x direction of magnetic field, and $\frac{dH}{dx}$ is the magnetic field gradient in the x direction. This function approximates the magnetic force on an object due to a known magnetic field gradient but does not account for the magnetization of the material. By assuming

that the magnetic material is superparamagnetic, the Langevin function can be used to approximate its magnetization. This function approximates the magnetic moment of superparamagnetic materials in an applied field [2.6, 2.26], and is denoted as:

$$L(\alpha) = \frac{M}{\phi M_d} = \coth \alpha - \frac{1}{\alpha} \quad (2.4)$$

where M is the magnetization of the particles, M_d is the bulk magnetic solid saturation moment of that material, ϕ is the volume fraction of nanoparticles. The parameter α is denoted as:

$$\alpha = \frac{\pi \mu_0 M_d D^3 H}{6 k_B T} = \alpha_0 H \quad (2.5)$$

where k_B is the Boltzmann's constant, T is temperature, D is the diameter of the nanoparticles, H is the magnetic field, and α_0 is a variable that donates α without the magnetic field. By rearranging Equation 2.4 to solve for magnetization and setting α as $\alpha_0 H$, the magnetization of nanoparticles can be described as:

$$M_{(x)} = \phi M_d \left(\coth \alpha_0 H - \frac{1}{\alpha_0 H} \right) \quad (2.6)$$

Values attained through this equation can be used to account for magnetization when approximating the magnetic force on a membrane under a known magnetic field.

However, to estimate the deflection of the membrane, the force must be divided by the area of the window opening to approximate the pressure. This approximation can be represented as:

$$\frac{F_m}{\pi a^2} = P_m \quad (2.7)$$

where F_m is the magnetic field applied to the membrane, a is the radius of the window open, and P_m is the pressure on the membrane due to the applied magnetic force. This pressure assumption allows the use of the generalized bulge equation to evaluate the magnetic deflection of a MNPC membrane, and in turn the volume production generated during deflection.

By assuming that the shape of the deflected membrane is hemispherical, the volume generated during membrane deflection can be approximated using the height and the radius of the window opening. The volume displaced during deflection of an edge clamped membrane can be depicted as in Figure 2.3.

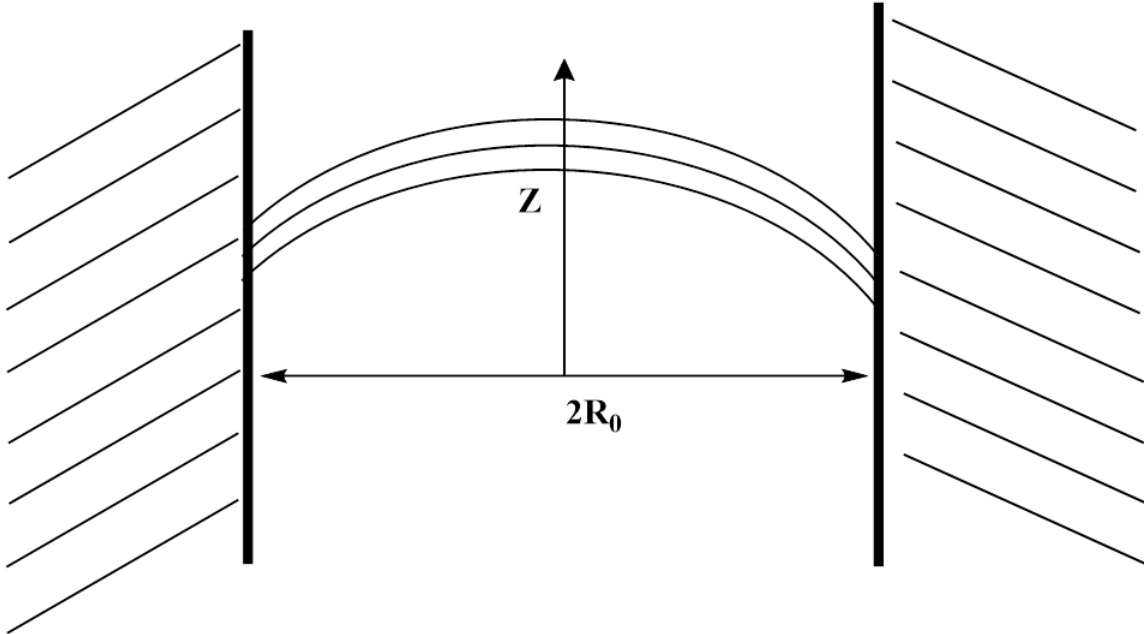


Figure 2.3: This caption is the side view of a deflected circular membrane that is bound at the edges. The variables in this image coincide with determining the displacement volume during membrane deflection.

This depiction can be expressed as

$$V = \frac{1}{3} \pi c R_0^3 \quad (2.8)$$

where V is the volume generated during membrane deflection and R_0 is the radius of the window that spans parallel from the center of the membrane to the edge [2.28]. The value c is denoted as

$$c = \frac{Z_0}{R_0^2} \quad (2.9)$$

where Z_0 is the maximum displacement of the membrane center [2.28]. With this approximation, the amount of volume displaced by the system can be estimated.

2.2.3 Bulge Testing Apparatus and Augmentations for Magnetic Deflection

The bulge testing system was originally designed to monitor the deflection of a membrane under applied pneumatic pressure (detailed in Appendix). Figure 2.4 shows the main components of this system.

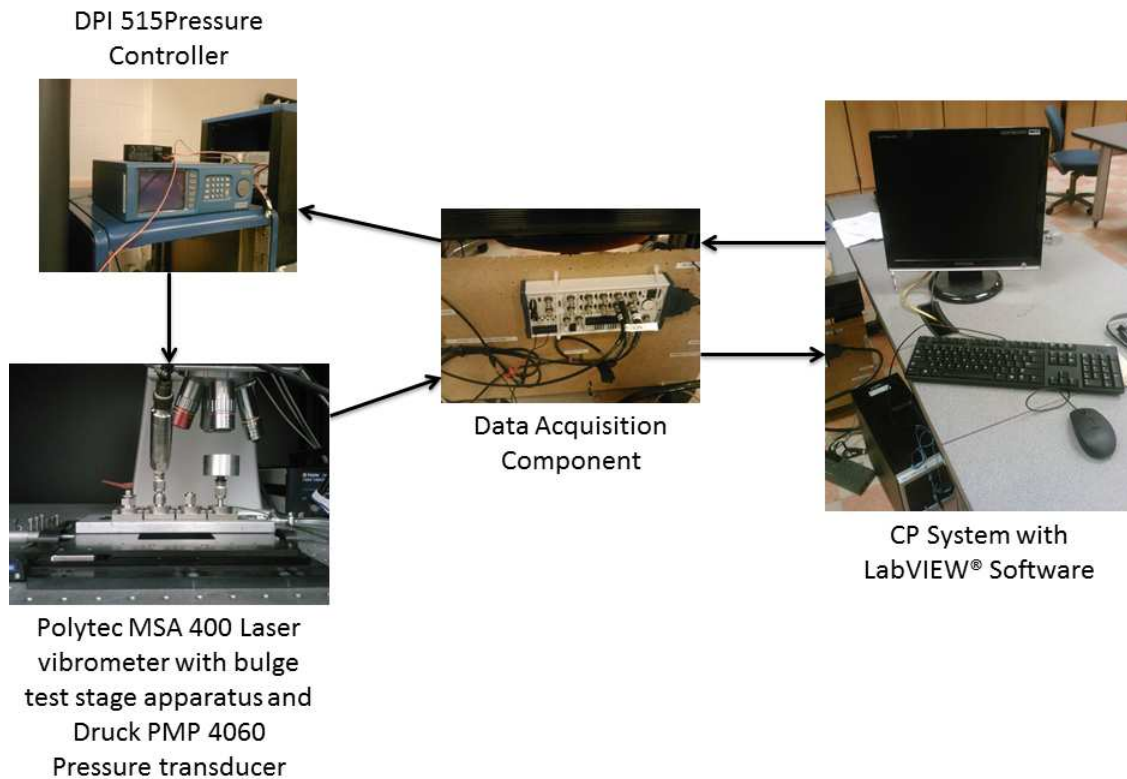


Figure 2.4: Clemson University bulge testing system with data flow schematic. Pressure values and rates are entered into the LabVIEW software, which is communicated to the pressure controller through the data acquisition component (DAQ). A pressure load is then applied to the testing stage, and both the laser vibrometer signal and the pressure signal from the transducer is relayed back to the software through the DAQ.

Alterations were made to the program and clamp of the bulge test system for more data acquisition and to account for magnetic deflection. The program was augmented by having it collect the data of all of the monitored parameters, and having that information storable in an adjacent program called NI DIAdem™ (for a more detailed discussion refer to the appendix section). The aluminum top clamp and non-magnetic 304 stainless steel screws used in the clamping system were replaced with a 1.1 mm poly lactic acid top clamp and brass polymer screws. This eliminated any magnetic effects during the magnetic deflection analysis due to the system setup, and allowed for closer placement of the actuating ring magnet.

2.3 Summary

In conclusion, the fabrication route for constructing MNPC membranes will affect the mechanical and structural properties. While the two identified routes can be used to produce membranes, the final application property requirements will dictate which route should be implemented. Modeling the nonlinear relationship between the pressure applied to a membrane and the attained deflection apex has been detailed in previous works. Using specific assumptions, this pressure deflection relationship could be used in describing the magnetic deflection of an MNPC membrane.

2.4 References

- [2.1] Francais, Dufour, Sarraute, Analytical Static Modelling and Optimization of Electrostatic Micropumps, *Journal of Micromechanics and Microengineering*, 7, (1997) 183-185.
- [2.2] Vlassak, *New Experimental Techniques and Analysis Methods for the Study of the Mechanical Properties of Materials in Small Volumes*, Stanford University, (1994).
- [2.3] Vinci, Vlassak, *Mechanical Behavior of Thin Films*, *Annual Reviews Materials Science*, 26, (1996) 33.
- [2.4] Hohlfelder, *Bulge and Blister testing of Thin Films and Their Interfaces*, Stanford University, (1998).
- [2.5] Pirmoradi, Cheng, Chiao, A Magnetic Poly(Dimethylsiloxane) Composite Membrane Incorporated with Uniformly Dispersed, Coated Iron Oxide Nanoparticles, *Journal of Micromechanics and Microengineering*, 20, (2010) 015032.
- [2.6] Fahrni, Prins, Van Ijzendoorn, Magnetization and Actuation of Polymeric Microstructures with Magnetic Nanoparticles for Application in Microfluidics, *Journal of Magnetism and Magnetic Materials*, 321, (2009) 1843-1850.
- [2.7] Evans, Fiser, Prins, Rapp, Shields, Glass, Superfine, A Highly Tunable Silicone-Based Magnetic Elastomer with Nanoscale Homogeneity, *Journal of Magnetism and Magnetic Materials*, 324, (2012) 501-507.
- [2.8] Mefford, Woodward, Goff, Vadala, St. Pierre, Dailey, Riffle, Field-Induced Motion of Ferrofluids through Immiscible Viscous Media: Testbed for Restorative Treatment of Retinal Detachment, *Journal of Magnetism and Magnetic Materials*, 311, (2007) 347-353.
- [2.9] Wang, Yao, Chen, Fang, Composite Elastic Magnet Films with Hard Magnetic Feature, *Journal of Micromechanics and Microengineering*, 14, (2004) 1321-1327.
- [2.10] Kennedy, Olson, Raupp, Moody, Bahr, Coupling Bulge Testing and Nanoindentation to Characterize Materials Properties of Bulk Micromachined Structures, *Microsystem Technologies*, 11, (2005) 298-302.
- [2.11] Huang, Lou, Tsai, Wu, Lin, Mechanical Properties of Polymer Thin Film Measured by the Bulge Test, *Thin Solid Films*, 515, (2007) 7222-7226.
- [2.12] Thangawng, Ruoff, Swartz, Glucksberg, An Ultra-Thin PDMS Membrane as a Bio/Micro–Nano Interface: Fabrication and Characterization, *Biomedical Microdevices*, 9, (2007) 587-595.
- [2.13] Song, Kim, Park, Three-Dimensional Hierarchically Organized Magnetic Nanoparticle Polymer Composites: Achievement of Monodispersity and Enhanced Tensile Strength, *Journal of Physical Chemistry C*, 112, (2008) 8.
- [2.14] Sarkar, Guibal, Quignard, Sengupta, Polymer-Supported Metals and Metal Oxide Nanoparticles: Synthesis, Characterization, and Applications, *Journal of Nanoparticle Research*, 14, (2012) 1-24
- [2.15] Fuhrer, Athanassiou, Luechinger, Stark, Crosslinking Metal Nanoparticles into the Polymer Backbone of Hydrogels Enables Preparation of Soft, Magnetic Field-Driven Actuators with Muscle-Like Flexibility, *Small*, 5, (2009) 383-388.

- [2.16] Li, Jia, Zhou, Hu, Cai, In Situ Hybridization to Chitosan/Magnetite Nanocomposite Induced by the Magnetic Field, *Journal of Magnetism and Magnetic Materials*, 306, (2006) 223-227.
- [2.17] Schlemmer, Betz, Berchtold, Rhe, Santer, The Design of Thin Polymer Membranes Filled with Magnetic Particles on a Microstructured Silicon Surface, *Nanotechnology*, 20, (2009) 255301.
- [2.18] Ramesh, Porel, Radhakrishnan, Polymer Thin Films Embedded with in Situ Grown Metal Nanoparticles., *Chemical Society reviews*, 38, (2009) 2646-2656.
- [2.19] Singh, Shirolkar, Limaye, Gokhale, Khan-Malek, Kulkarni, A Magnetic Nano-Composite Soft Polymeric Membrane, *Microsystem Technologies*, 19, (2012) 409-418.
- [2.20] Kennedy, Olson, Raupp, Moody, Bahr, Coupling Bulge Testing and Nanoindentation to Characterize Materials Properties of Bulk Micromachined Structures, *Microsystem Technologies*, 11, (2005) 298-302.
- [2.21] Jiang, Markutsya, Pikus, Tsukruk, Freely Suspended Nanocomposite Membranes as Highly Sensitive Sensors, *Nature Materials*, 3, (2004) 721-728.
- [2.22] Klapperich, Komvopoulos, Pruitt, Nanomechanical Properties of Polymers Determined from Nanoindentation Experiments, *Journal of Tribology* 123 (2001) 624.
- [2.23] Xiang, Chen, Vlassak, Plane-Strain Bulge Test for Thin Films, *Journal of Materials Research*, 20, (2011) 2360-2370.
- [2.24] Vlassak, Nix, A New Bulge Test Technique for the Determination of Young's Modulus and Poisson's Ratio of Thin Films, *Journal of Materials Research*, 7, (2011) 3242-3249.
- [2.25] Reid, Deformation and Adhesion of Thin Metallic Films on Flexible Substances, *Materials Science and Engineering* , Clemson Univeristy, (2011).
- [2.26] Coey, Rhen, Dunne, Mcmurry, The Magnetic Concentration Gradient Force—Is It Real?, *Journal of Solid State Electrochemistry*, 11, (2007) 711-717.
- [2.27] Xu, Su, Development, Characterization, and Theoretical Evaluation of Electroactive Polymer-Based Micropump Diaphragm, *Sensors and Actuators A: Physical*, 121, (2005) 267-274.
- [2.28] Hall, Apperson, Crozier, Xu, Richards, Bahr, Richards, A Facility for Characterizing the Dynamic Mechanical Behavior of Thin Membranes for Microelectromechanical Systems, *Review of Scientific Instruments*, 73, (2002) 2067.

CHAPTER THREE

MATERIALS FOR CONSTRUCTING MNPC MEMBRANES AND CHARACTERIZATION METHODS

The materials chosen for this system are crosslinked PDMS for the polymer matrix and IONPs as the magnetic filler. Prior studies confirmed that both materials have acceptable biocompatibility and useful properties for bio-micropump applications [3.1, 3.3-3.7]. The bulk mechanical properties of crosslinked PDMS has been referenced as having a low elastic modulus, which reduces the amount of force needed for a membrane of this material to deflect [3.1, 3.7-3.10]. To fabricate PDMS with iron oxide particles, we used the published method by Pirmoradi et al. as the starting point for this study [3.1]. As stated previously, the *ex-situ* method effects the nanoparticle agglomeration within the film and sets a lower limit on attainable thickness. Though, it can be also viewed that some of the groups that used *ex-situ* method lacked the ability to properly stabilize the nanoparticles in the mixture prior to crosslinking the system. Nevertheless in Pirmoradi et al.'s study, the agglomeration size within the material was on average less than $1.6 \pm 0.25 \mu\text{m}$ in diameter, resulting in a membrane no thinner than $35 \mu\text{m}$ to be formed [3.1]. However, for our study the thickness of the membrane was arbitrarily chosen to be around 100-200 μm , which negates the limiting effects of the method.

3.1 Nanoparticle Synthesis

The IONP synthesis process used in this study were determined by comparing two methods, Hyeon et al. and Huber (unpublished works). The Hyeon synthesis method was performed by adding 1 mL (7.60 mmol) of iron pentacarbonyl to a mixture of 7.15 mL

(22.8 mmol) oleic acid and 50 mL of octyl ether in a 100 ml three neck round bottom flask under nitrogen purged at 100 °C. The solution was mixed using a magnetic stir bar and heating was controlled using a Glas-Col heating mantle and a J-Chem temperature control box and thermal couple. The solution was allowed to equilibrate at 100 °C for 30 min and then increased to reflux at a rate of 3.33 °C/min. The solution was allowed to equilibrate for 1 hour and then removed from heat to cool for 30 min. After the allotted time 1.964 g (7.60 mmol) of 1,2 hexadecandiol was added to the solution and then left to stand at 130 °C. The solution was allowed to equilibrate at 130 °C for 30 min and then increased to reflux again at a rate of 3.33 °C/min. The solution was allowed to stand for 1 hour and then removed from heat to cool in air.

Nanoparticles synthesized through the Huber method were fabricated via thermal decomposition of 6.445 g (18.25 mmol) of Fe(III) acetylacetonate was mixed with 90 mL (285.17 mmol) of oleic acid in a 500 mL three-neck round bottom flask. The solution was stirred at 400 revolutions per minute (RPM) using an IKA RW 20 D S1 overhead stirrer. The solution was allowed to stand in a metal heating bath for 15 min. at 150 °C under nitrogen flow (1 L/min.). The bath was then heated at 5 °C per min. to 350 °C and held for approximately five hours. After the time had expired, the flask was quickly removed from the metal bath and left to cool to room temperature in air.

Cleaning the particles produced by both methods was performed by adding 45 mL of acetone to five mL of the reaction solution in a centrifuge tube. The solution was then mixed vigorously by using a combination of a Vortexer (Scientific Industries Inc. Vortex-Genie 2 no.G560) for 5 min. and then sonicated (Bransonic Ultrasonic Cleaner 2510R-

DTH) for 2 min. This was done with the intent of removing excess ligand and other unreacted material from the particle solution. The particles were then precipitated by using a Thermo Scientific Sorvall Legend x1 centrifuge at a speed of 10k RPM held for five min. The precipitant was dispersed in 5 mL of hexane by using the vortexer for two min. and sonication for 30 seconds. This wash procedure was done three times on the entire batch of each method before their collection. The particles synthesized via Huber method were collected in a 500 mL one-neck round bottom flask and the particles synthesized via Hyeon method were collected for characterization in 4-5 scintillation vials. The solution produced by the Huber method was dried using a Heidolph Laborota 4000 efficient rotovap at 40 °C at 180 RPM and suspended in 200 mL of hexane for nanoparticle characterization and storage.

3.2 MNPC and Metallic Film Processing

The magnetic nanoparticle membranes in this study were synthesized using a methods in literature [3.1, 3.7]. The nanoparticle solution (20 mL with an iron concentration of 3.43 mg/mL) was sonicated for five min. and then added drop wise to 1.8 g Sylgard 184 PDMS base component in a scintillation vial through a 5 mL microliter pipet. The new solution was mixed for five min. at 1500 RPM using the overhead mechanical stirrer, sonicated in the Bransonic Ultrasonic Cleaner 2510R-DTH sonication bath for ten min., and dried under reduced pressure at 50 °C at max RPM under vacuum. This was done until the solution became viscous and this process was repeated until the desired concentration of nanoparticles was reached within the vial. Sylgard 184 PDMS

(0.36 g) part B was added to the solution then mixed and bath sonicated using the previous parameters and instruments. The solution was then dried under reduced pressure at room temperature at 180 RPM under vacuum, and then poured onto a five μm thick polymethyl methacrylate (PMMA) release layer atop of a 304 stainless steel substrate polished to a mirrored finish from Stainless Supplies Inc. The PMMA release layer used in these experiments was synthesized prior to pouring the PDMS/IONP samples by thoroughly mixing ~ 0.7 grams of PMMA in ten mL of chloroform, and then spin coating three mL of the solution onto the stainless steel disc using the Specialty Coating System Spin Coater P6204-A at 700 RPM for 60 seconds. The steel disc and release layer were then placed in the Shel Lab 1400E vacuum oven for two hours at approximately 120°C under vacuum to ensure that excess chloroform was removed. The PDMS/IONP samples were spin coated at ~ 1000 RPM for 30 seconds and then placed in the vacuum oven at 116°C under vacuum for three hours. Next, the film was removed from the oven and two samples were harvested for structural analysis. The film was then plasma cleaned using the Harrick-Plasma PDC-001 for one min. at max power and then sputtered upon using an augmented Kurt J. Lesker company sputtering system with processing parameters of $\sim 9.9\text{--}9.7 \times 10^{-7}$ Torr base pressure, and 1.5×10^{-2} Torr processing pressure. Titanium (10 nm) was deposited as an adhesion layer after ten min. under 100 W DC plasma followed with gold (100 nm) after 28 min. under 160 W RF. A thin (2 μm in thickness) layer of pure PDMS was spin coated atop of the gold film and left to sit in the vacuum oven for 48 hours at room temperature under vacuum. The resultant film

system is depicted in Figure 3.1. This entire construction process was used to ensure that consistency was held for each weight percentage.



Figure 3.1: This depiction shows how the layers of the film system will result after the MNPC construction process is completed. It should be noted that only the gold and MNPC layers will be used for bulge testing and magnetic deflection testing.

3.3 Sample Preparation for Characterization.

The nanoparticles and MNPC membranes were structurally characterized. Nanoparticle characterization was conducted using the Hitachi TEM H 7600 transfer electron microscope (TEM) to determine particle size, and Thermo Scientific Inductive coupling plasma mass spectroscopy X series 2 (ICP-MS) to measure concentration of iron. The MNPC membrane was characterized to determine distribution of particles

(Olympus Optical BX60F-3 optical microscopy (OM)), and roughness (a Mikro Precision Instruments Wyko Nt-2000 topographical white light Profilometry).

To analyze the nanoparticles, an aliquot of 50 μL from the concentrated stock suspension of IONPs in hexane was taken and then dispersed with 20 mL of additional hexane. Of this diluted suspension, an aliquot of 10 μL was added to a TEM grid and allowed to dry. The grid was imaged with magnifications varying from 50,000 to 100,000 \times . The captured images were used to determine the size and shape of the nanoparticles. ICP-MS was used to determine the concentration of the bulk suspension by taking 0.5 mL of the bulk solution and adding 20 mL of hexane. Ten μL of this suspension was taken and digested it with 418 μL of nitric acid. The resulting solution is diluted to 14 mL for a desired 2 wt. % of nitric acid and then measured following a calibration curve of standard solutions varying in iron concentration. Determining the concentration of nanoparticles of the overall reaction is important in determining the conversion efficiency of the reaction and to ascertain if the desired amount of nanoparticles were met. Figure 3.2 depicts how samples for each test were harvested for each weight percentage sample set.

was used for each image analysis to determine cluster size. In the event cluster size could not be determined by OM. TOPO was conducted on three 1.7 cm² samples per weight percentage. One of the samples came from the prior study with OM and two were harvested from the edge and in between. A total of seven scans per weight percentage were taken from center to edge to determine the average thickness of each film.

3.4 Mechanical and Magneto-Mechanical Characterization

Once membranes were made, the following characterization methods were used to identify the mechanical properties and magnetic response of these membranes. Nanoindentation was used to measure the elastic moduli of the membranes. Ten indents were initially taken on one 1.7 cm² sample per weight percentage using a Hysitron TS 70 TriboScope® series using a Nano-DMA™ transducer. The Ti-047(04) 90° conical tip was used with a constant frequency of 45 Hz during the indentation. Twenty steps with 100 cycles per step were taken with a starting and ending quasi-static load of 75-175 μN with a dynamic load of .75 μN. These parameters were set so that the penetration depth is less than 450 nm for a total time of 1.01 minutes for each indent. Bulge testing and magnetic deflection were conducted using the custom built system discussed earlier. For bulge testing, each sample was cycled for four times through a pressure range of ±0.1 PSI at a rate of 0.01 PSI per second. For magnetic deflection, the magnetic source was a 0.1 tesla ring magnet with dimensions of one inch outer diameter, 0.5 inches inner diameter, and 0.25 inches in thickness. The properties of this magnet were approximated for one direction was placed on top of a 1.1 mm thick plastic clamp to deflect each

sample three times for ~10000 seconds each time. Pressure and deflection during this evaluation is monitored and record via the LabVIEW program.

3.5 References

- [3.1] Pirmoradi, Cheng, Chiao, A Magnetic Poly (Dimethylesiloxane) Composite Membrane Incorporated with Uniformly Dispersed, Coated Iron Oxide Nanoparticles, *Journal of Micromechanics and Microengineering*, 20, (2010) 015032.
- [3.2] Park, Kang, Son, Park, Lee, Kim, Kim, Noh, Park, Bae, Park, Hyeon, Monodisperse Nanoparticles of Ni and NiO: Synthesis, Characterization, Self-Assembled Superlattices, and Catalytic Applications in the Suzuki Coupling Reaction, *Advanced Materials*, 17, (2005) 429-434.
- [3.3] Fuhrer, Athanassiou, Luechinger, Stark, Crosslinking Metal Nanoparticles into the Polymer Backbone of Hydrogels Enables Preparation of Soft, Magnetic Field-Driven Actuators with Muscle-Like Flexibility, *Small*, 5, (2009) 383-388.
- [3.4] Evans, Fiser, Prins, Rapp, Shields, Glass, Superfine, A Highly Tunable Silicone-Based Magnetic Elastomer with Nanoscale Homogeneity, *Journal of Magnetism and Magnetic Materials*, 324, (2012) 501-507.
- [3.5] Pirmoradi, Jackson, Burt, Chiao, A Magnetically Controlled Mems Device for Drug Delivery: Design, Fabrication, and Testing, *Lab on a Chip*, 11, (2011) 3072.
- [3.6] Schlemmer, Betz, Berchtold, Ruhe, Santer, The Design of Thin Polymer Membranes Filled with Magnetic Particles on a Microstructured Silicon Surface, *Nanotechnology*, 20, (2009) 255301.
- [3.7] Fahrni, Prins, Van Ijzendoorn, Magnetization and Actuation of Polymeric Microstructures with Magnetic Nanoparticles for Application in Microfluidics, *Journal of Magnetism and Magnetic Materials*, 321, (2009) 1843-1850.
- [3.8] Wang, Yao, Chen, Fang, Composite Elastic Magnet Films with Hard Magnetic Feature, *Journal of Micromechanics and Microengineering*, 14, (2004) 1321-1327.
- [3.9] Liu, Sun, Sun, Bock, Chen, Thickness-Dependent Mechanical Properties of Polydimethylsiloxane Membranes, *Journal of Micromechanics and Microengineering*, 19, (2009) 035028.
- [3.10] Song, Kim, Park, Three-Dimensional Hierarchically Organized Magnetic Nanoparticle Polymer Composites: Achievement of Monodispersity and Enhanced Tensile Strength, *Journal of Physical Chemistry C*, 112, (2008) 8.

CHAPTER FOUR

RESULTS, DISCUSSION, AND CONCLUSION

4.1 Determining Method to Synthesizing Easy to Model Nanoparticles

The thermal decomposition method of synthesizing nanoparticles detailed in Hyeon et.al. was used [4.1]. The assumed nanoparticles this method produced were monodisperse maghemite particles instead of the magnetite particles. This method was altered by substituting the oxidizing agent, dehydrated trimethylamine N-oxide $(\text{CH}_3)_3\text{NO}$, with the reducing agent, 1,2 hexadecandiol, at the same molar ratio. This reaction was performed using an increased molar ratio (by a factor of 5), which yielded black nanoparticles. However, the reproducibility of this synthesis proved resulting batches of nanoparticles with large sizes and differing geometries as seen in Figure 4.1.

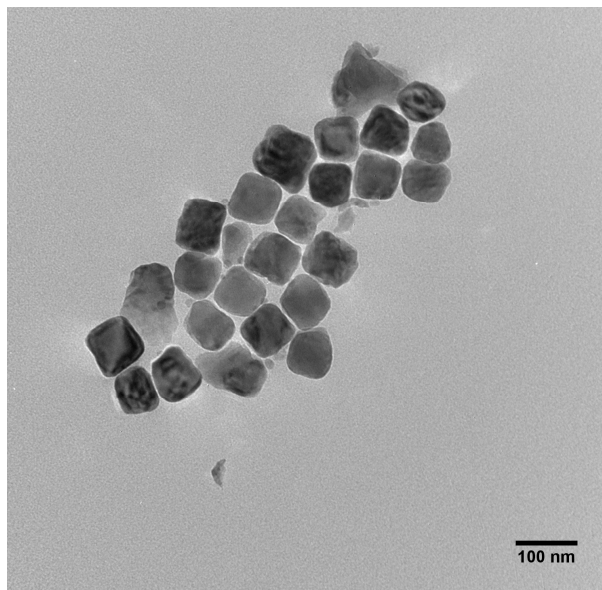


Figure 4.1: TEM of nanoparticles synthesized using Hyeon et al. method, which displays particles of varying geometries.

However, using the synthesis outlined in Chapter 2 the nanoparticles derived were spherical and monodispersed in shape as seen in Figure 4.2.

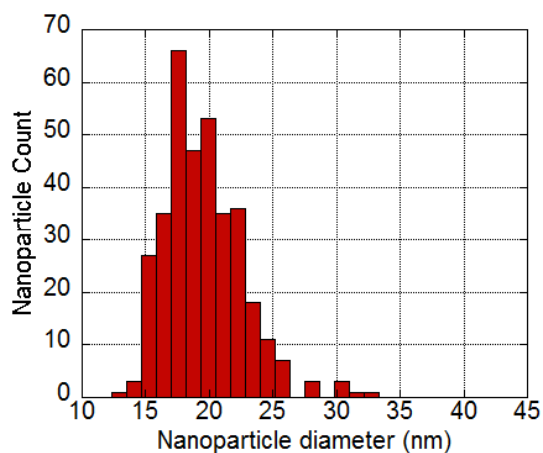
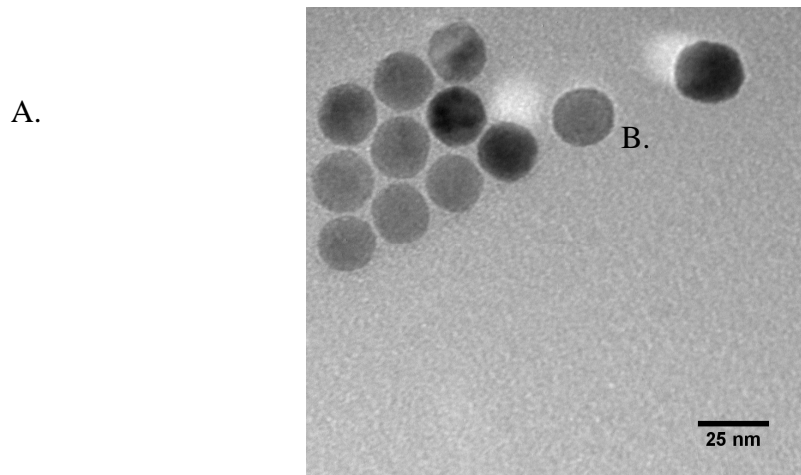


Figure 4.2: TEM of nanoparticles derived using the Sandia National Laboratory (unpublished research). The left (a.) shows shape and size uniform amongst the particles, while the right (b.) shows the nanoparticle distribution.

In order to attain the amount of nanoparticles necessary for producing MNPC membrane systems, two nanoparticle synthesis reactions were conducted. The target weight amount and particle diameter was approximately 1.28 g of IONPs with a core

diameter of 25 nm. Both reactions synthesized a combined amount of 1.733 g of nanoparticles with a mean core diameter of 24.6 nm with a standard deviation of ± 3.1 nm. The TEM and size histogram of the nanoparticles can be seen in figure 4.3.

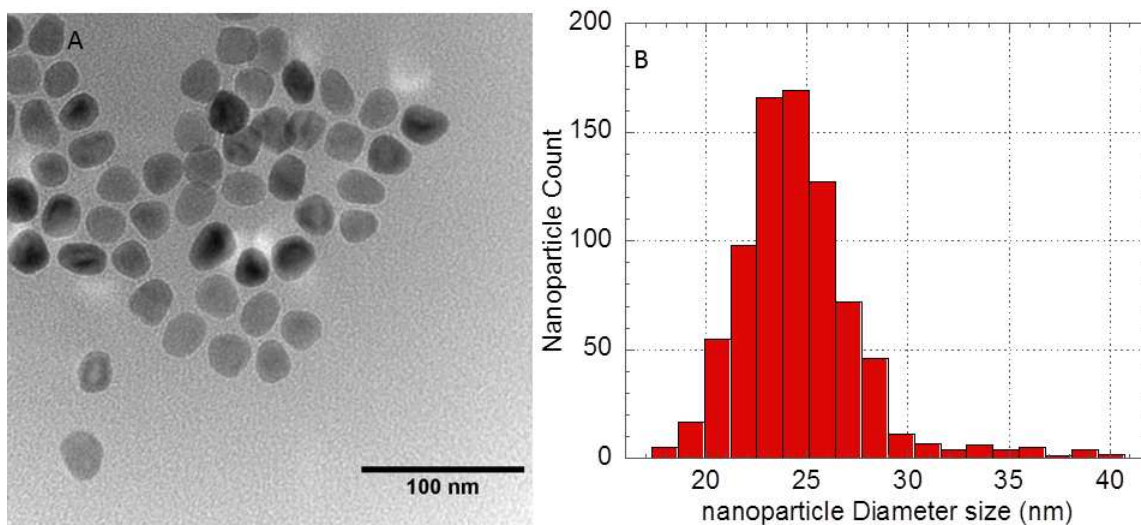


Figure 4.3: A.) A representative TEM image and b.), the nanoparticle size analysis histogram of the combined nanoparticle batches synthesized.

When comparing Figures 4.2 to 4.3a the shape of the particles of Figure 4.3 is more ellipsoidal than circular. A possible reason for this discrepancy relates to the time used to synthesize. The reactions conducted for constructing films with nanoparticles of uniform size in this thesis were scaled up by a factor of six from the method used to synthesize the nanoparticles in Figure 4.2. However, the time used for this synthesis was almost two hours longer due to the size of reaction vessel. Over this time period, smaller particles can dissolve and redeposit on to larger particles, known as the Ostwald ripening [4.2]. This can form polydisperse nanoparticles in time dependent nanoparticle syntheses, which is a plausible explanation for the odd particle shapes and size distribution.

4.2 Determining Method for MNPC Membrane Processing

The following section outline the process improvements made during this project to improve MNPC membrane fabrication. Preliminary methods involved using polystyrene petri dishes as substrates during spin coating and film curing. Polystyrene dishes were initially used due low economic cost for the quality of film roughness being produced. PDMS films would not adhere to the petri dish's nanometer rough surface, but the substrate would deform during the curing process of the system as seen in Figure 4.4.

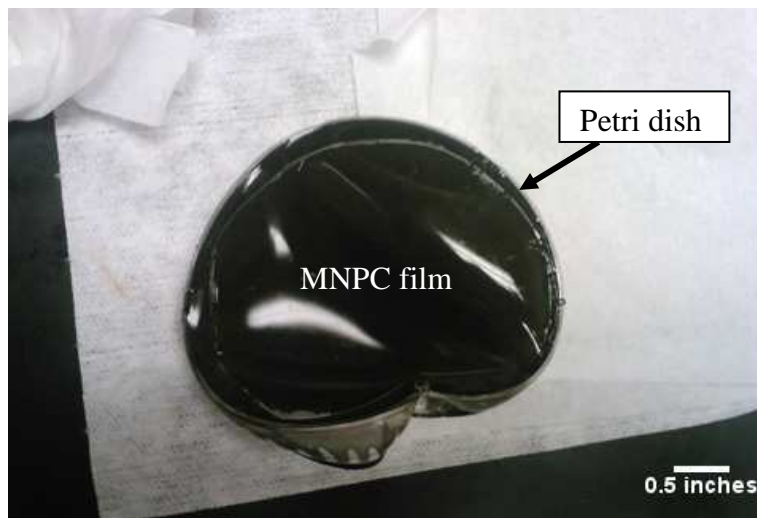


Figure 4.4 MNPC film system on petri dish after the curing process.

Thus, there was a need to find a material that would offer the same low roughness, but would not buckle during the curing process. PMMA coated mirrored steel was introduced as a way to support the MNPC film curing process and would not buckle, which can be viewed in Figure 4.5.

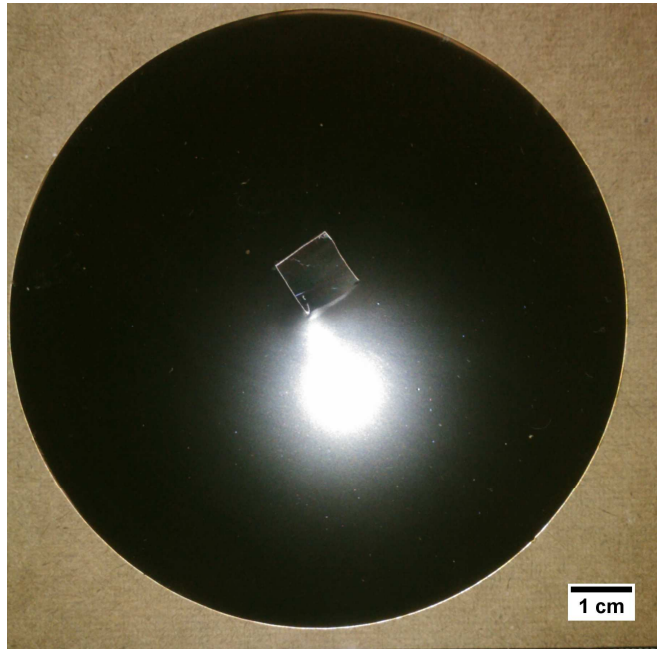


Figure 4.5. Image of a MNPC membrane on top of a mirrored steel substrate. The substrate allows for higher temperatures during the MNPC crosslinking process without deformation.

This substrate was proven to be successful during the crosslinking process, and was used in the attempt of synthesizing films with higher weight percent of nanoparticles.

4.3 Analysis and Comparison of Particle Clustering in MNPC Film Systems

Two samples from 0 wt. % and 5 wt. % film systems were harvested in the manner detailed in Chapter 3. The bright field optical images of the unloaded and loaded samples displayed expected results for each film system. As shown Figure 4.6, the 5 wt. % sample clearly shows clustering within the film with an average particle diameter of $2.26 \pm 1.23 \mu\text{m}$ and average particles per cluster $1.54 \times 10^6 \pm 2.5 \times 10^6$.

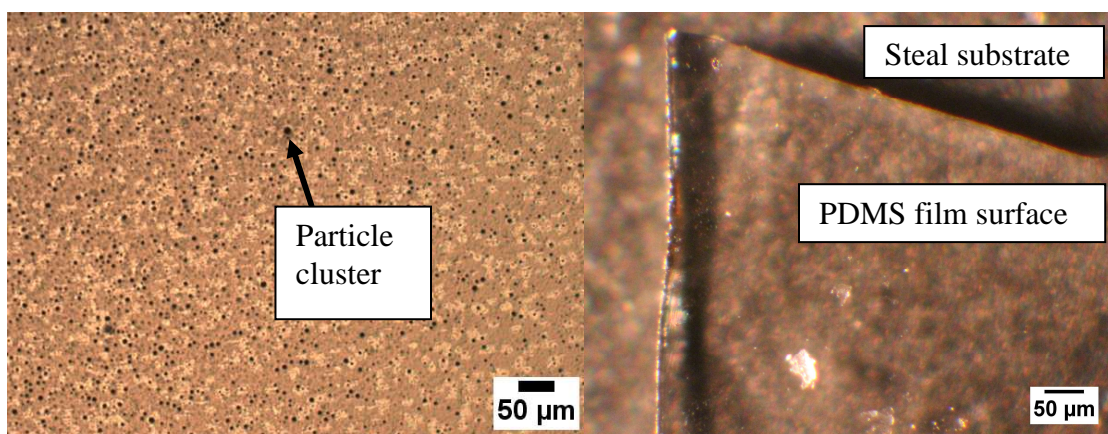


Figure 4.6: Nanoparticle loaded and unloaded film systems. Left, is the 5 wt. % film system. Right, is the 0 wt. % film system.

The average cluster size determined by OM was consistent with literature [4.3], which justified that further cluster analysis using a higher powered microscope was not necessary.

4.4 Analysis of the Metallic Layer System

When preparing the sample for bulge testing or magnetic deflection, the thin metallic film on top of the sample can fail as seen in Figure 4.7. This component of the system is very important because, it is the conduit in measuring deflection using the laser vibrometer. If the reflective film cracked or buckled during the sample preparation, this would introduce error into the deflection measurement. To minimize the effects of sample preparation on the metallic layer an additional PDMS layer was spin coated on top of the gold layer [4.4].

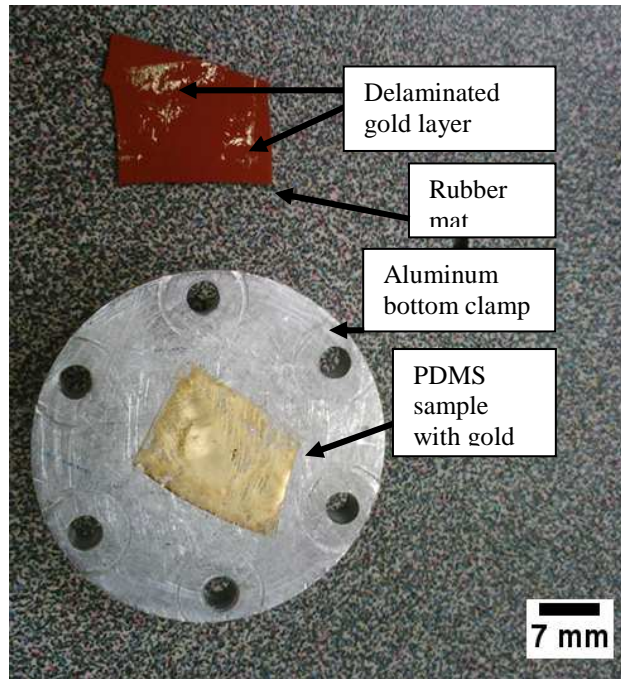


Figure 4.7: Metallic film that failed as a result of sample preparation.

This top layer is then discarded during sample preparation with minimal damage to the metallic film as seen in Figure 4.8. The resultant films are sufficiently reflective to be analyzed by bulge testing.

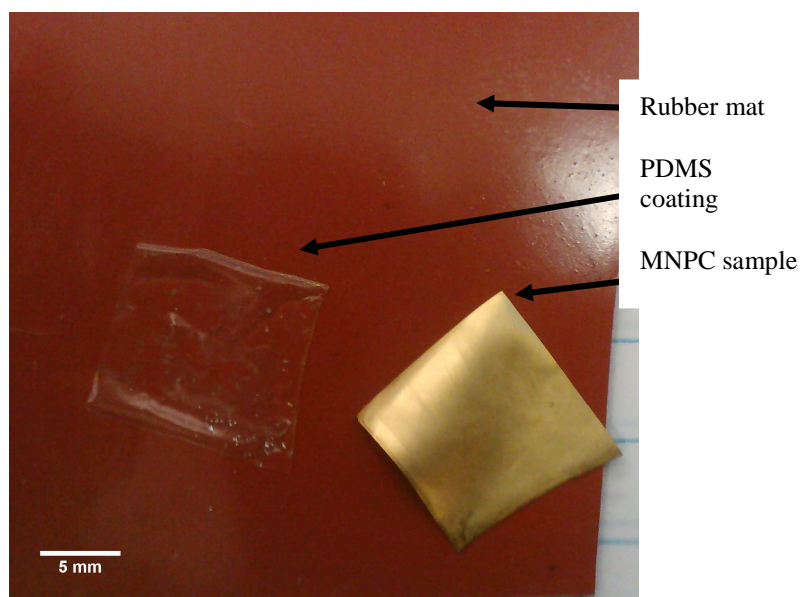


Figure 4.8: Example of a film system with minimal damage after sample preparations.

4.5 Thickness Analysis of the Film Systems

After receiving a metallic layer and polymer protective coating, films were harvested in the manner described in Chapter 3, and the thickness of each film was analyzed accordingly. The thickness of the unloaded to the loaded samples for the set spin-coating parameters, varied drastically. The thickness from center to edge of the unloaded sample varied from 48-49 μm , however the loaded sample varied from 108-183 μm in thickness.

4.6 Preliminary Mechanical Characterization Results of MNPC Membrane via

Nano-DMA™

Prior to characterizing the MNPC membranes bulge testing, a preliminary experiment was conducted. This experiment was to prove that the elastic modulus of

these materials changed with increasing concentrations of IONPs and that this difference can be monitored using Nano-DMA™. Samples containing nanoparticle weight percentages of 0 wt.% and a 5 wt. % were used and sample sizes of 100 sample points of elastic modulus data was taken.

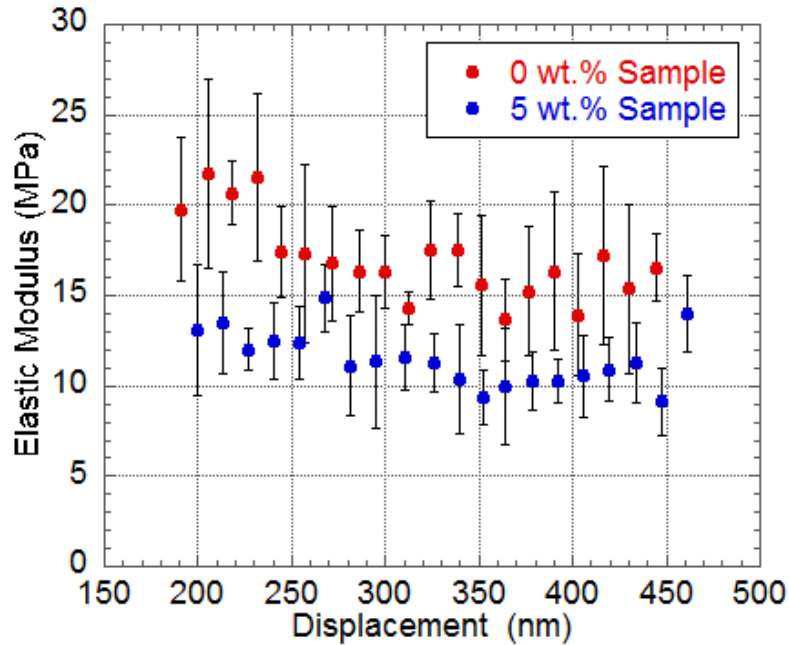


Figure 4.9: Nano-DMA™ data of the 5 wt. % and 0 wt. % samples

The mean and standard deviation were calculated using Minitab software and a paired T-test was performed using Minitab software to determine if the mean elastic modulus values for each sample were equivalent. The null hypothesis for this test was that the elastic modulus for both samples was statistically the same. (note: If the p-value of this test is less than the alpha value the null hypothesis is rejected.) It was concluded that the elastic moduli of the 0 wt. % and 5 wt. % samples were 15.2 ± 3.4 MPa and 10.2 ± 2.7 MPa, respectively. The finding of the T-test concluded that, at a 95% confidence interval

(alpha value equal to 0.05), the p-value was 0.000. This suggests that the modulus of each sample is statistically different and the elastic modulus decreasing as particle concentration in the film increases was observed. This observed mechanical property trend was similar to that of materials found in literature fabricated using the ex-situ methodology

4.7 Results of Pressure Deflection Testing of the MNPC Membranes

For pressure deflection, the data acquired between loaded and unloaded samples was used to determine residual stress of the film system. The data was fitted to an offset equation with all the known parameters, which is depicted by Equations 4.1

$$P_0 = -P^* + A(x_0 - x^*) + B(x_0 - x^*)^2 \quad (4.1)$$

where P_0 is the approximated pressure at the origin, P^* is the experimentally found pressure data, x_0 is the calculated displacement offset, x^* is the experimentally found displacement data, A is the parameter component that contains residual stress, and B is the parameter component that contains elastic modulus. This technique was used to account for offsets in the pressure and displacement data due to error in the bulge test system [4.5].

When the elastic modulus measured by Nano-DMA™ technique was used, the data did not fit Equation 4.1. Setting the equation so that the modulus is unknown fits the data as seen as the trend line in Figure 4.10. This fit determined an average modulus

of 2.29 ± 0.31 MPa for the unloaded samples and 1.04 ± 0.20 MPa for the loaded. The residual stress for each system was 13.6 ± 9.0 KPa and 29.4 ± 18.3 MPa for the unloaded and loaded samples, respectively.

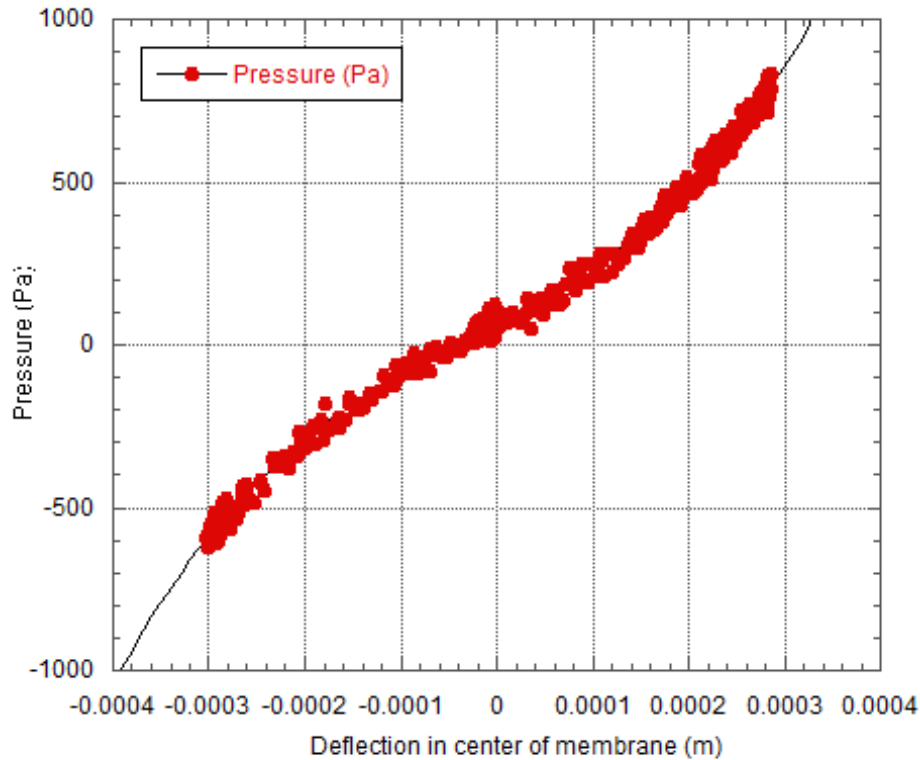


Figure 4.10: Representative bulge testing data with curve fit line without using known Young's modulus values

4.8 Results of Magnetic Deflection Testing of the MNPC Membranes

For magnetic deflection of the 5 wt. % 0 wt. % samples, the data did not correlate to the expected hypothesis. The ring magnet used in this test possesses a magnetic field strength of ~ 0.06 T in the center of the ring at 1.1 mm away from the ring surface, which was determined using a Metrolab Three-axis Hall magnetometer. This was the lowest distance at which the samples were tested. Using the original assumptions, the model

predicted that the deflection of the loaded membrane to be $.162 \mu\text{m}$ and $0 \mu\text{m}$ for the 5 wt. % and 0 wt. % samples respectively. However, it was observed by magnetic deflection that the membranes deflected $17.36 \mu\text{m}$ and $-2.13 \mu\text{m}$ for the 5 wt. % and 0 wt. % samples respectively. The suspected reason for this is that certain assumptions within the current mathematical model are violated while testing with the current magnetic deflection setup, and that an uncounted force was applied to the system. After an analysis of the test set up for magnetic deflection, the use of a ring magnet to deflect the MNPC system was not suitable for a comparison to the model. It was suitable for validating whether membrane deflection is detectable using the vibrometer system due to its high magnetic field and field gradient. However, the field and field gradient geometry of the ring magnet is not represented in the current model under consideration.

The model accounts for a system that applies a magnetic field and gradient in one direction and assumes that the force is consistent across the area of the membrane. This would imply that the way in which a magnetic and pneumatic force deflects a MNPC membrane is equal. This would be the case for cylindrical, permanent magnets where, at certain distances from its poles, the magnetic field and field gradient remains constant across the lateral directions.

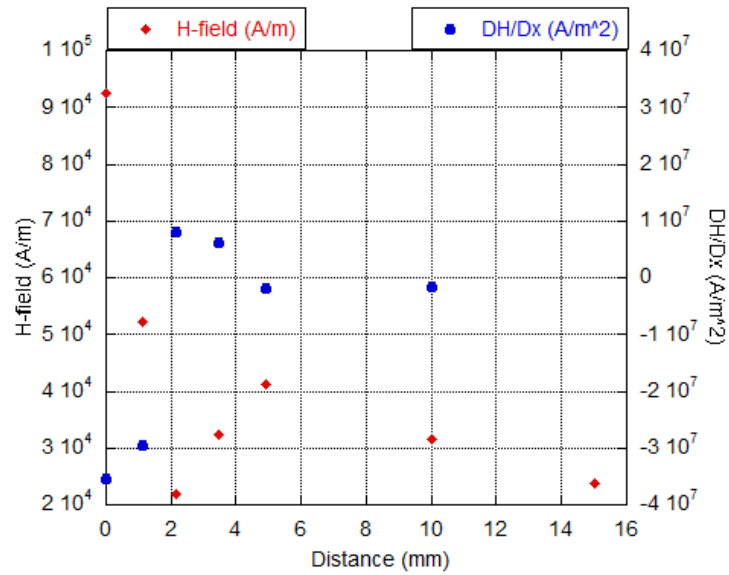


Figure 4.11: H-field profile of the center of the ring magnet over a distance of 0 to 15 mm.

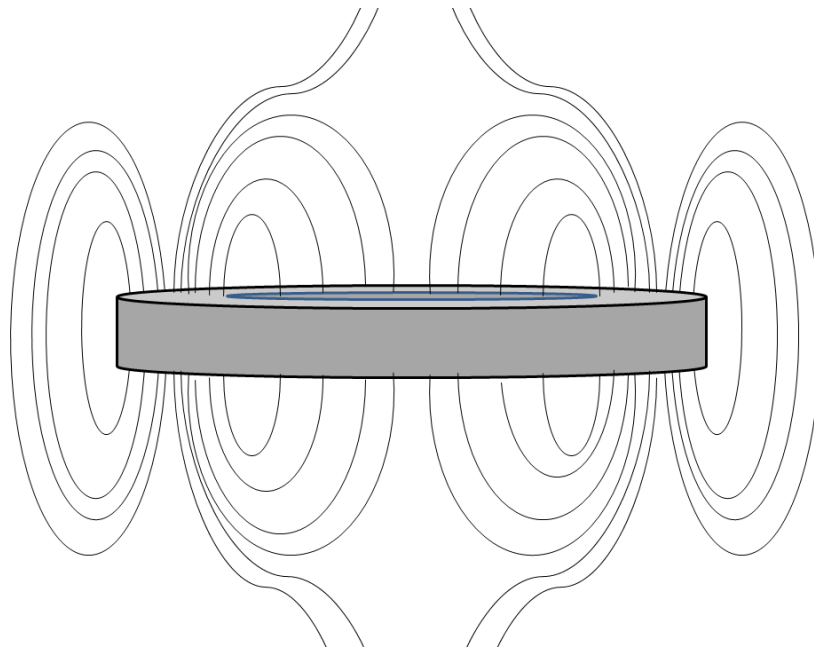


Figure 4.12: The depiction of the magnetic field for an axially magnetized ring magnet.

Ring magnets can be magnetized in a variety of anisotropies. For our experiments the type of ring magnet used was axially magnetized through the thickness of the material

as depicted in the H-field profile of Figure 4.11. Notice how the magnetic field changes between 2 and 6 mm; this is expected for ring magnets magnetized as suggested. Figure 4.12 is an illustration of a ring magnet magnetized as described based off Lin and Yang et al. fluid element analysis [4.6, 4.7]. For a certain distance away from the ring magnet, the field and field gradient will change in the lateral direction. This means that the membrane was affected both laterally and vertically at the center. As stated earlier, the field strength used to test at the center of the membrane was approximately 0.06 tesla; however the field strength increases from the center of the ring to the internal edge. With this in mind, the earlier assumption that the force is equal across the membrane is violated. The interpretation could then be that, during magnetic deflection with a ring magnet at said distance, the membrane will experience more force towards the edges than at the center. This is best depicted by Figure 4.13, where the thicker arrows represent a larger force experienced at that location.

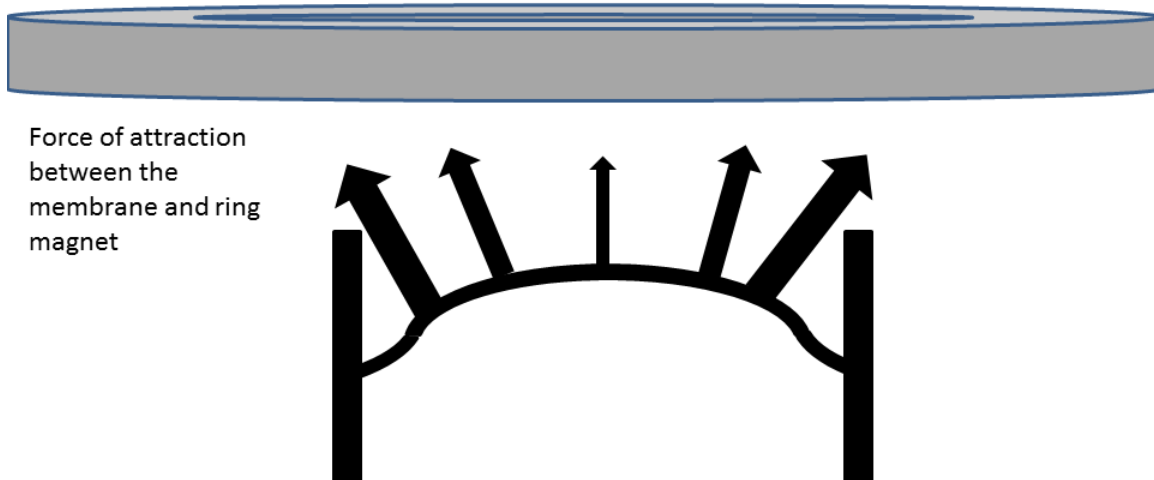


Figure 4.13: Depiction of how a ring magnet is theorized to effects the MNPC membranes when the magnetic field gradient is greater in the lateral direction compared to the normal

The negative deflection of the 0 wt % sample was not predicted by the model nor expected through conventional wisdom. A possible reason for this is due to the residuals ferrous material on the testing stage. Though the testing clamp was redesigned to replace most of the materials of the current testing clamp, what was not replaced was the ferrous material of the testing stage (see appendices for better stage description). The top clamp connects to the stage through a cast iron screw component. By placing the magnet on the top clamp will introduce a magnetic field within close proximity of the cast iron component. This magnetic field would exert a downward force on the clamp system, causing the membrane to buckle during testing. In essence, comparing the current test set

up using the pneumatic model defined in earlier chapters neither validates the current hypothesis nor disproves it. Further augmentation using a material with a magnetic field that follows the assumptions of the model would be beneficial.

4.9 Results of Processing MNPC Films with Higher Particle Concentrations

Using particles produced by the Sandia method resulted in synthesizing films only 0 and 5wt. % at a crosslinking ratio of 3:1 (B:C). The prescribed method outline in Chapter 3 to construct the 20 wt. % sample failed to crosslink film upon the surface of the substrate. What resulted was a polymer melt without a ridged shape that coagulated into small patches across the surface of the substrate as seen in Figure 4.14.



Figure 4.14: MNPC film sample that did not crosslink after deposition, evident by the visual appearance of the mirrored steel substrate.

As a result, additional crosslinker was added to the remaining planned samples, changing the ratio from 5:1 to 3:1.

4.9.1 Analysis of Uncrosslinked MNPC Systems

An investigation was conducted to confirm why film systems 10-20 wt. % failed to crosslink. An extraction was performed on the 15 wt.% sample by scrapping .461 g of the uncrosslinked sample into a 50 ml centrifuge tube and performing an additional wash step outlined in section 2.2.1. The sample was then separated from the supernatant by decanting the liquid and drying by flowing nitrogen gas over the sample. The sample was reweighed to estimate the percent of weight loss due to washing. As a result the sample weight after the extraction was .406 g, which amounted to 12% weight loss.

The yellow supernatant was then collected, centrifuged, and dried with nitrogen gas. The resultant residue was collected and analyzed with an Agilent Technologies Cary 600 Series FTIR with the Cary 620 Microscope and the Cary 680 Spectrometer and the PIKE technologies MIRacle diamond ATR attachment. The resultant spectra of the sample was compared to the spectra of oleic acid and iron oleate to confirm if an excess of either chemical was present in the sample as seen in Figure 4.15.

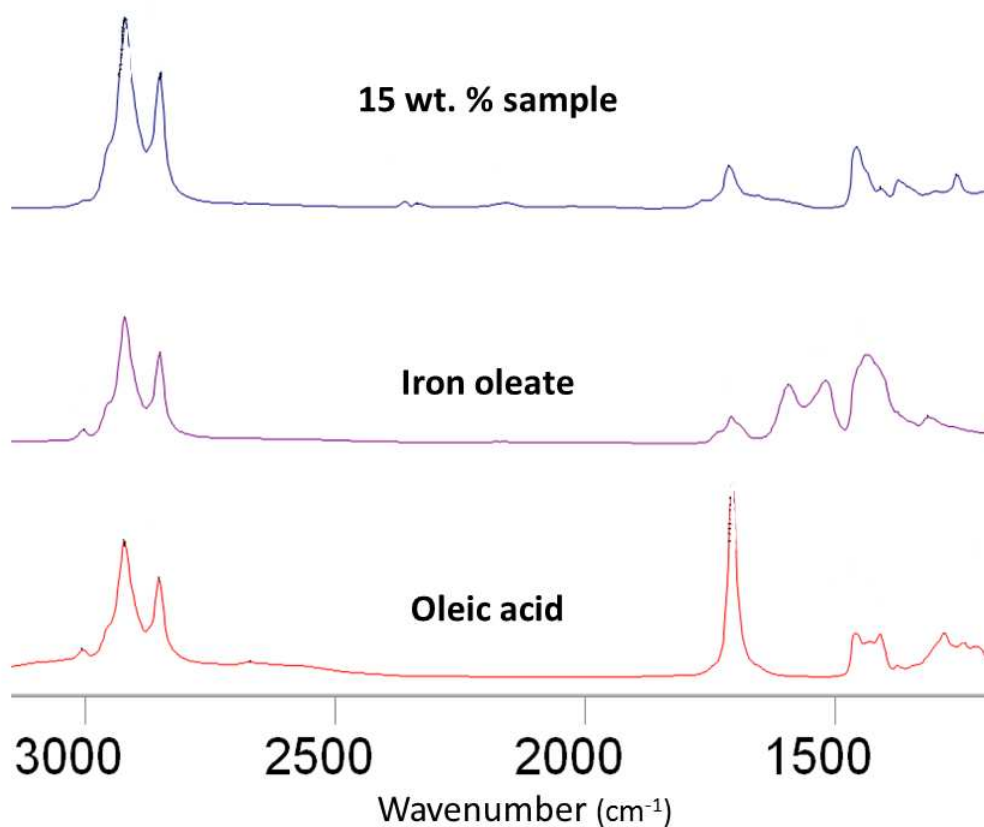


Figure 4.15: FTIR finger print region comparison of the 15 wt. % sample, iron oleate, and oleic acid.

As it appears, the spectra of the sample lack the two peaks between 1600 and 1500 cm⁻¹ that distinguishes iron oleate from oleic acid [4.8]. The plausible explanation for why the films above 10 wt. % did not crosslink was due to the presence of an excess amount of oleic acid that could have interfered with gelation [4.3, 4.9]. It is perceived in previous works that oleic acid interferes with the platinum catalyst used within the system to crosslink [4.3, 4.9]. However, it is perception that oleic acid directly affects the crosslinking density of the system by reacting with the methylsilane sites in the backbone of the polymer chain. This PDMS elastomer kit uses alkene functionalized end-groups to

react with methyl silane sites to gel forming the crosslinked polymer system. Oleic acid is a monounsaturated fat with an alkene group that could react with these sites, thus inhibiting the system's ability to crosslink by reducing the amount of sites available. By affecting the methyl silane reaction sites the polymer's ability to gel decreases or not occur. This could have consequences that would affect the elastic modulus of the resulting films if the excess oleic acid is not completely washed from the particles, and the presence on the particles should also be of concern

4.10 Conclusions

In summary, the prescribed method for synthesizing MNPC films was successful at constructing a system contain up to 5 wt. % of magnetic nanoparticles. OM confirmed the presence of clustering within the 5 wt. % loaded system, which was comparable to literature. The thickness of the loaded and unloaded systems varied drastically when comparing the disc samples to each other.

Preliminary mechanical characterization of the 0 and 5 wt. % samples determined that the moduli for each sample are significantly different. It was also shown that the depression in modulus trend consistent with literature when characterized by Nano-DMA™. However, using these moduli to approximate the residual stress in bulge testing resulted in inaccurate values. When comparing the mathematical model to experimental data, the amount of magnetic deflection expected underestimates the true value by almost two orders of magnitude for the 5 wt. % system.

When comparing the assumptions of the model to the experimental setup for testing magnetic deflection the model does not account for lateral differences in the magnetic field and field gradient. This implies that the model is not agreeable for the experimental setup and a better approximation would be retrofitting the testing system to follow the assumptions of the model. For the 0 wt. % system, magnetic deflection averaging approximately 2 μm was observed which also not accounted for the model. Constructing film systems containing IONPs more than 5 wt. % was not successful. This was due to excess oleic acid within the system that was not removed using the prescribed washing method.

4.11 References

- [4.1] Hyeon, Lee, Park, Chung, Na, Synthesis of Highly Crystalline and Monodisperse Maghemite Nanocrystallites Without a Size-Selection Process, *Journal of the American Chemical Society*, 123, (2001) 12798-12801.
- [4.2] Teng, Yang, Effects of Surfactants and Synthetic Conditions on the Sizes and Self-Assembly of Monodisperse Iron Oxide Nanoparticles *Journal of Materials Chemistry*, 14, (2004) 774.
- [4.3] Pirmoradi, Cheng, Chiao, A Magnetic Poly (Dimethylesiloxane) Composite Membrane Incorporated with Uniformly Dispersed, Coated Iron Oxide Nanoparticles, *Journal of Micromechanics and Microengineering*, 20, (2010) 015032.
- [4.4] Lewis, Material Challenge for Flexible Organic Devices, *Materials Today*, 9, (2006) 38-45.
- [4.5] Hohlfelder, Bulge and Blister testing of Thin Films and Their Interfaces, Stanford University, (1998).
- [4.6] Lin, Valentine, Ring-Shaped NdFeB-Based Magnetic Tweezers Enables Oscillatory Microrheology Measurements, *Applied Physics Letters*, 100, (2012) 201902.
- [4.7] Yang, Wang, The Stable Levitation of an Iron Ball over a Ring Magnet, *Journal of Superconductivity and Novel Magnetism*, 25, (2011) 421-425.
- [4.8] Bronstein, Huang, Retrum, Schmucker, Pink, Stein, Dragnea, Influence of Iron Oleate Complex Structure on Iron Oxide Nanoparticle Formation, *Chemistry of Materials*, 19, (2007) 3624-3632.
- [4.9] Fahrni, Prins, Ijzendoorn, Magnetization and Actuation of Polymeric Microstructures with Magnetic Nanoparticles for Application in Microfluidics, *Journal of Magnetism and Magnetic Materials*, 321, (2009) 1843-1850.

CHAPTER FIVE

FUTURE RESEARCH DIRECTIONS TO ENHANCE RESULTS

While progress has been made to experimentally understand the structure-performance relationships of PDMS-IONP membranes, this work should be expanded before being utilized to design and fabricate MNPC membranes to integration into an operational biomicropumps. This chapter will highlight the necessary steps to improve the membrane processing, magneto-mechanical characterization, and the comparison between *in-situ* and *ex-situ* synthesized materials presented in previous chapters. Section 4.1 will highlight suggested alterations to MNPC synthesis presented in Chapter 2 and how it affected the mechanical properties presented in Chapter 3. This section will also consider new material synthesis methods to reduce agglomeration within MNPC membranes. In Section 4.2, improvements will be suggested to improve the accuracy of the experimental mechanical characterization methods and pressure deflection model.

5.1 Possible Methods to Improve Current MNPC Structure through Fabrication

The membranes fabricated using the *ex-situ* synthesis method presented in Chapter 3 had a similar relationship between nanoparticle loading and elastic modulus to those reported earlier [5.1, 5.2]. Other groups had suggested the reasons for this decrease could be related to: an interfacial absorption issue between the polymer chains and the nanoparticle surface [5.2], or an interference with the curing ability of the polymer matrix [5.1, 5.2]. Nanoparticles that are synthesized in organic solutions contain an organic

coating for aggregation suppression and stability [5.3]. Introducing particles (i.e., ligand coated nanoparticles) of this type into a polymer matrix reduces the possibility of interfacial absorption of the polymer matrix to the nanoparticle surface. This can affect the mechanical properties of the composite by not reinforcing the system when a stress is applied [5.2, 5.4].

The other postulate, which is the interference with the curing ability during MNPC membrane processing, was theorized due to the reaction kinetics involved in crosslinking this type of PDMS. The matrix material used in both this and previous studies is Sylgard 184™ [5.1, 5.2, 5.5], which utilizes the reaction between methylsilane in the polymer backbone and the alkene end-groups of the polymer chain [5.6]. This reaction becomes competitive when a material containing unsaturated hydrocarbon is introduced during the synthesis. Depending on the amount of this material may cause the crosslinking density of the resulting polymer matrix to be less than intended or not crosslinked.

In this study, specific reasons for the decrease in elastic modulus with increasing particle loading were not experimentally determined. This study did show that increasing the amounts oleic acid present could change the stiffness by preventing crosslinking. This influence of oleic acid was highlighted previously by Fahrni et al. [5.1]. A study to quantify the amount of free oleic acid (acid that is not bound to the nanoparticle) could be used to identify its effects on the system's stiffness. Proper material purification can be used to remove any remaining free oleic acid from the nanoparticle solution [5.7, 5.8]. Thermogravimetric analysis TGA can be performed to calculate the amount of oleic acid

on the nanoparticle surface [5.7, 5.8]. From that one only needs to add an aliquots series of oleic acid with a constant amount of nanoparticles to confirm the effects of acid on membrane properties. The benefits of this study would allow for the finding of a potential upper limit amount of oleic acid a membrane system could have without affecting the crosslinking. If correct, this could possibly be another avenue of control over the mechanical properties of the MNPC membrane system.

Nanoparticle agglomeration is a consistent issue when using the *ex-situ* fabrication method to synthesize MNPC membranes [5.1, 5.2, 5.9]. This study confirms that using physical means to reduce nanoparticles agglomeration within a polymer matrix will reduce agglomerates to that of 1-2 μm . This becomes a problem for membrane systems that need a thickness thinner than a micron because the nanoparticles would not achieve uniform dispersion throughout the system. A way to combat this would be to use an *in-situ* MNPC fabrication method [5.9, 5.10]. This method has been shown to reduce the nanoparticle agglomeration within the composite, and also achieve higher particle concentrations within the system. Thus, the use of this method would address the issues of failure to increase nanoparticle concentration in the system and the particle clustering issues.

Switching from an *ex-situ* to an *in-situ* fabrication method could improve the as-fabricated structure of the PDMS-IONP membranes. However, materials of this nature demonstrate an enhancement of mechanical properties as the nanoparticle concentration in the system increases [5.9]. A comparison between processes would offer better insight into the strengths and weaknesses of the materials derived from each synthesis type. An

experimental path to achieve this would be to alter the Evan et al. fabrication method to imbed coated nanoparticles into the matrix [5.9]. This can be performed by synthesizing IONPs through co-precipitation and splitting the batch for different functionalization routes. One part of the batch can be partially functionalized with oleic acid before crosslinking, while the other batch would follow a procedure similar to Evans et al. Both systems would use the amine functionalized PDMS as the matrix material. Using this process will offer better control over slight material variation found in literature, while maintaining both systems conceptual differences.

Another path of interest would be combining the *in-situ* and *ex-situ* methods as a possible means of controlling the system's mechanical properties. The combination of these methods would seek to increase the contents of the magnetic component in the MNPC system, while depressing or not affecting the material's stiffness. This could be achieved by varying the process stated in the previous paragraph to combine both sets of particles into a single matrix before crosslinking. Using these methods in combination could be the foundation for MNPC materials with extreme amounts of magnetic particle loading and controlled mechanical properties.

5.2 Enhancing the Current Magnetic-Mechanical Characterization Capabilities at

Clemson University

By improving the methods outlined in Chapter 2, the influence of the magnetic field on the membrane shape, deflection resolution and measurement repeatability could be quantitatively defined. The magnetic field and field gradient should be altered by the

raising and lowering a ring magnet. As discussed in Section 3.6.2 the direction of force on the center of the membrane will change depending on the distance between the membrane and ring magnet. Below a distance of 5 mm, the field gradient in the lateral direction becomes greater than the direction normal to ring magnet axial surface. Thus the membrane experience a force that is pulls it more lateral than normal. This force on the membrane is dissimilar to the force applied pneumatically by the bulge system, thus it was not possible to directly compare the deflection response. Also, the magnetic properties of the magnet are fixed to certain distances away from the sample, so in order to change the magnetic field and field gradient the clamping system must be changed to compensate. To improve this system, future students could (1) design a new way to move the permanent magnet to set distances from the membrane or (2) use an electromagnet instead of a permanent magnet.

For designing a system where the mobility of a permanent magnet is augmented, a future student would need to make a few adjustments to the current setup. The current clamping system would need to become detachable from the pressure deflection system to be able to compare the membrane response to both stimuli. A testing stage would need to be constructed above the current apparatus to hold the clamped membrane in place, while the permanent magnet is moved vertically underneath. The mobility of the magnet would be dependent upon a micrometer, allowing for better measurements of distance. These system changes are based on Singh et al. apparatus [5.5], and could allow for the testing of permanent magnets with different geometric shapes. The design complexity of this system should be simplistic and be able to measure magnetic deflection accurately.

To design an apparatus that controls the magnetic field and field gradient applied to a membrane, without a mobile permanent magnet, would need to integrate a solenoid coil into the system. The coil would be composed of enameled copper wire, which is commercially available, and could be housed within the clamping system. The magnetic field produced by a solenoid coil is determined by the applied current, permeability of free space, and number of turns along the coil. The distance of the coil to the sample and the number of turns in the coil would be fixed, while the current applied to the system would be variable. This concept was previously designed by Lederer et al. [5.11], where a magnetic micropump system was constructed using an integrated coil for actuation. This idea could give rise to better control over the magnetic field resolution achievable during magneto-mechanical characterization.

5.3 References

- [5.1] Fahrni, Prins, Ijzendoorn, Magnetization and Actuation of Polymeric Microstructures with Magnetic Nanoparticles for Application in Microfluidics, *Journal of Magnetism and Magnetic Materials*, 321, (2009) 1843-1850.
- [5.2] Pirmoradi, Cheng, Chiao, A Magnetic Poly(Dimethylsiloxane) Composite Membrane Incorporated with Uniformly Dispersed, Coated Iron Oxide Nanoparticles, *Journal of Micromechanics and Microengineering*, 20, (2010) 015032.
- [5.3] Wang, Wong, Teng, Lin, “ Pulling ” Nanoparticles into Water : Phase Transfer of Oleic Acid Stabilized Monodisperse Nanoparticles into Aqueous Solutions of R - Cyclodextrin, *Nano Letters*, 3, (2003) 1555-1559.
- [5.4] Bokobza, Rapoport, Reinforcement of Natural Rubber, *Journal of Applied Polymer Science*, 85, (2002) 2301-2316.
- [5.5] Singh, Shirolkar, Limaye, Gokhale, Khan-Malek, Kulkarni, A Magnetic Nano-Composite Soft Polymeric Membrane, *Microsystem Technologies*, 19, (2012) 409-418.
- [5.6] Dow Corning Corporation, in, Dow Corning Corporation, (2005) 1-8.
- [5.7] Shen, Gee, Tan, Pellechia, Greytak, Purification of Quantum Dots by Gel Permeation Chromatography and the Effect of Excess Ligands on Shell Growth and Ligand Exchange, *Chemistry of Materials*, 25, (2013) 2838-2848.
- [5.8] Davis, Qi, Witmer, Kitchens, Powell, Mefford, Quantitative Measurement of Ligand Exchange on Iron Oxides Via Radiolabeled Oleic Acid., *Langmuir: The ACS Journal of Surfaces and Colloids*, 30, (2014) 10918-10925.
- [5.9] Evans, Fiser, Prins, Rapp, Shields, Glass, Superfine, A Highly Tunable Silicone-Based Magnetic Elastomer with Nanoscale Homogeneity, *Journal of Magnetism and Magnetic Materials*, 324, (2012) 501-507.
- [5.10] Fuhrer, Athanassiou, Luechinger, Stark, Crosslinking Metal Nanoparticles into the Polymer Backbone of Hydrogels Enables Preparation of Soft, Magnetic Field-Driven Actuators with Muscle-Like Flexibility, *Small*, 5, (2009) 383-388.
- [5.11] Lederer, Heinisch, Hilber, Jakoby, Electromagnetic Membrane-Pump with an Intergrated Magnetic Yoke, *IEEE Sensors*, (2009) 532-537.

APPENDIX

Appendix A

Bulge Testing System Operation

A.1 Bulge Testing System Development

The bulge test system, Figures A.1 and A.2, was originally designed by Nathan Mitchell and later improved by Julie Reid [A.1].

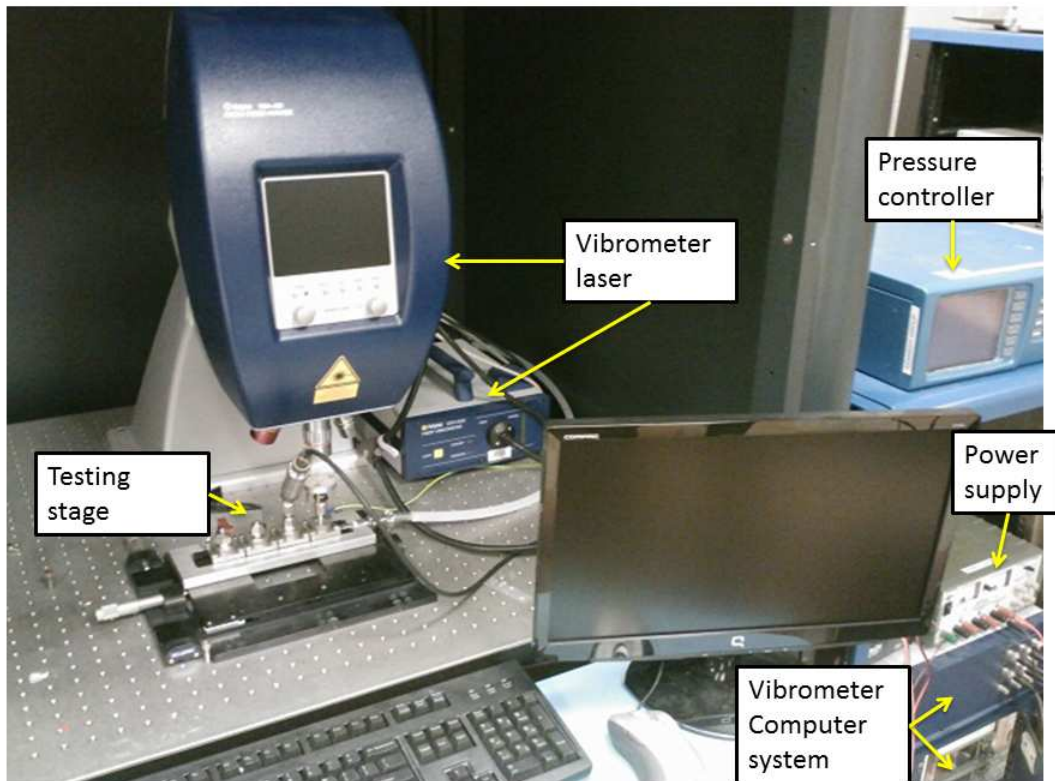


Figure A.1: The vibrometer computer and pressure controls

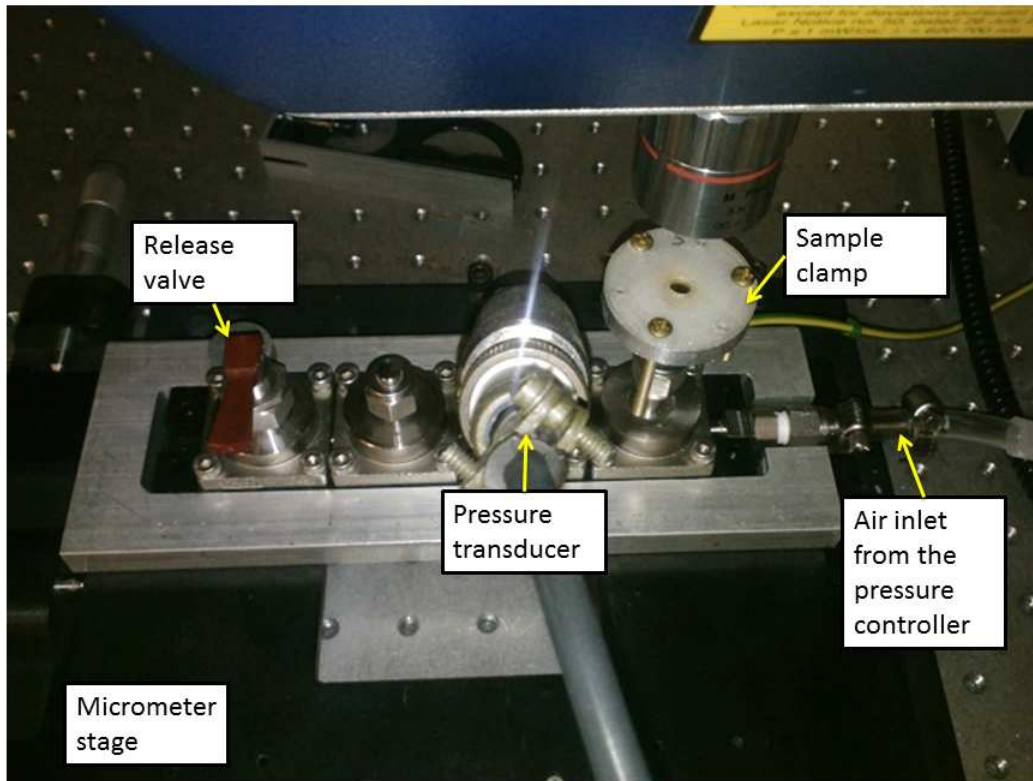


Figure A.2: The components of the bulge testing stage where the deflection measurements are taken.

This system currently monitors the deflection of membranes at a point (normally the center of the membrane), the pneumatic pressure from the Druck pressure controller, and the measured pneumatic pressure below the membranes as read by a pressure transducer as a function of time. The laser vibrometer signal strength (which signifies that amount of light that is reflected back to the detector of the vibrometer) is also monitored [A.1].

The current program, collects voltage readings to calculate the membrane center height (in μm), the pressure from the transducer (in psi), and data rate (one point per 0.01 sec) [A.1]. The previously reported resolution each component is as follows:

- The maximum height that can be detected is $\pm 500 \mu\text{m}$ [A.1].
- The precision of the pressure controller can apply pressure to the system with an error of $\pm .003 \text{ PSI}$ [A.2].
- The resolution of the pressure transducer has a measurement error of $\pm .036 \text{ PSI}$, which is one order of magnitude higher than the controller [A.2, A.3].

This system is unique because it was designed to test samples produced by roll-to-roll techniques and these sheets are clamped to create membranes. To prepare a sample, the flat membrane is superglued into an aluminum die with a circular opening using Locatite 401 instant adhesive [A.1]. The work in this thesis always used a 6 mm diameter that was then mounted over the pressure inlet of the bulge testing stage to be evaluated [A.1]. The top part of the clamp, made of 3D printed poly lactic acid produced at Clemson University's Rich laboratory, allowed for magnetic deflection measurements within a distance of 1.1 mm to the membrane.

Measurement Error and Limitations within Bulge Testing System

Error during the measurement has been known to occur due to slight changes in the membrane geometry when preparing samples. Before gluing samples into the clamp, the membrane must be flat and devoid of wrinkles. The top clamp must also be tighten to where the sample will not slip, but not over tighten to were the membrane could buckle as seen in previous work [A.1]. The consequence of having a wrinkled or buckled

membrane violates an assumption when applying the bulge testing equation, as described above [A.4-A.6]. If excess glue is used, it will bleed into the window opening and create a thin film on the bottom of the sample. This leads to error during the analysis by slightly altering the geometry of the membrane. If not enough glue is applied, the sample will be able to slip during the evaluation, also causing an alteration in the geometry of the membrane [A.1]. The effect of membrane slip during bulge testing is represented in Figure A.3 below.

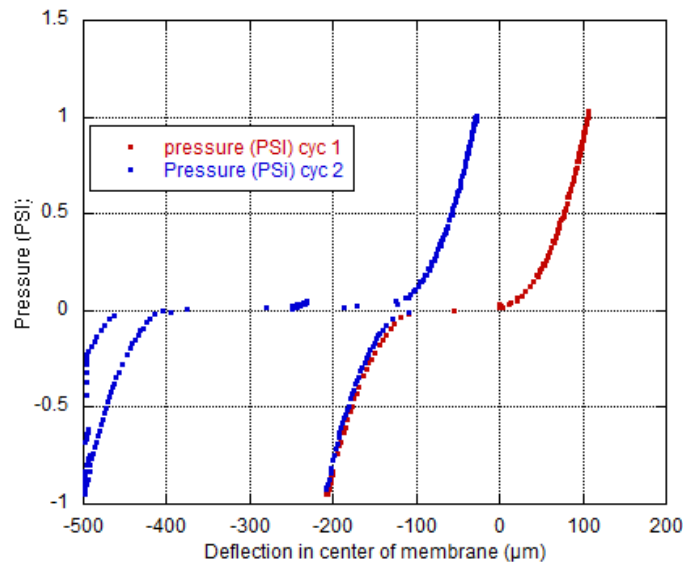


Figure A.3: This is a representative graph of how slip appears in the data collected from bulge testing. The sample used for this representation went through two pressure cycles of ± 1 PSI

Consistent bulge testing data should be symmetric around the origin when positive and negative pressure is applied to the system, while also overlaying each pressure cycle. In Figure A.3 the inconsistency in the data occurs as a form of a discontinuity during pressure cycling, thus causing the data from cycle one and two not to overlay. It is during this discontinuity that the sample housed in the test clamping system is believed to have slipped during testing, which would cause large variations in the concluded moduli and

residual stress values. However, if the sample is fashioned to the clamping system correctly then the data should appear as shown in Figure 2.1 of Chapter 2. Taking special precautions to avoid these oversights during sample preparation will reduce error in the pressure/deflection data due to the process.

Using Clemson University's Improved Bulge Testing System

System Setup: System Initiation

- 1) Turn on air flow leading to the DPI 515 (pressure controller) and the air table.
 - a) Ensure that the pressure gauge at the main manifold reads 40 PSI.
 - b) Ensure that the pressure gauge at the junction point reads 35 PSI.
- 2) Turn on vacuum pump, DPI 515, MSA I400 vibrometer controller and laser, and the power supply for the PMP 4060 (pressure transducer).
- 3) Access the laser vibrometer system software.
- 4) Turn on the adjacent computer.
- 5) Initiate the LabVIEW program "Akeem's recalibrated xy.vi" and activate the DIAdem™ software using the computer directly across from the bulge testing stage, see Figures A.4 and A.5 for appearance.
- 6) Let system stand for at least one hour before using to allow for the vibrometer laser to thermally equalize.

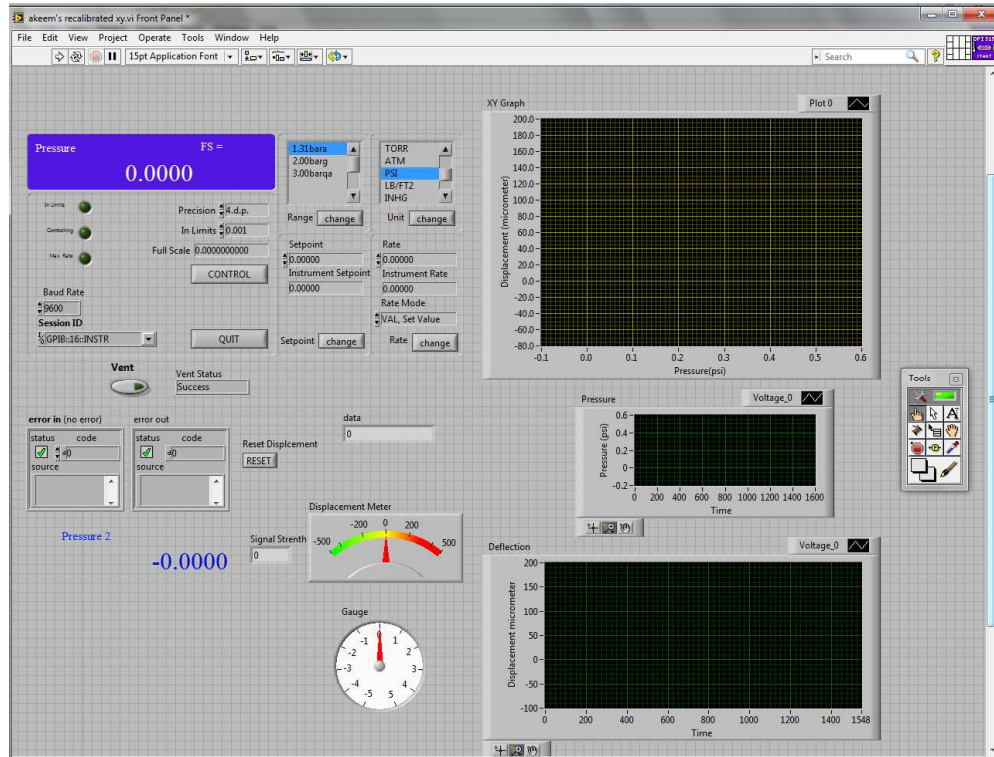


Figure A.4: LabVIEW program front panel

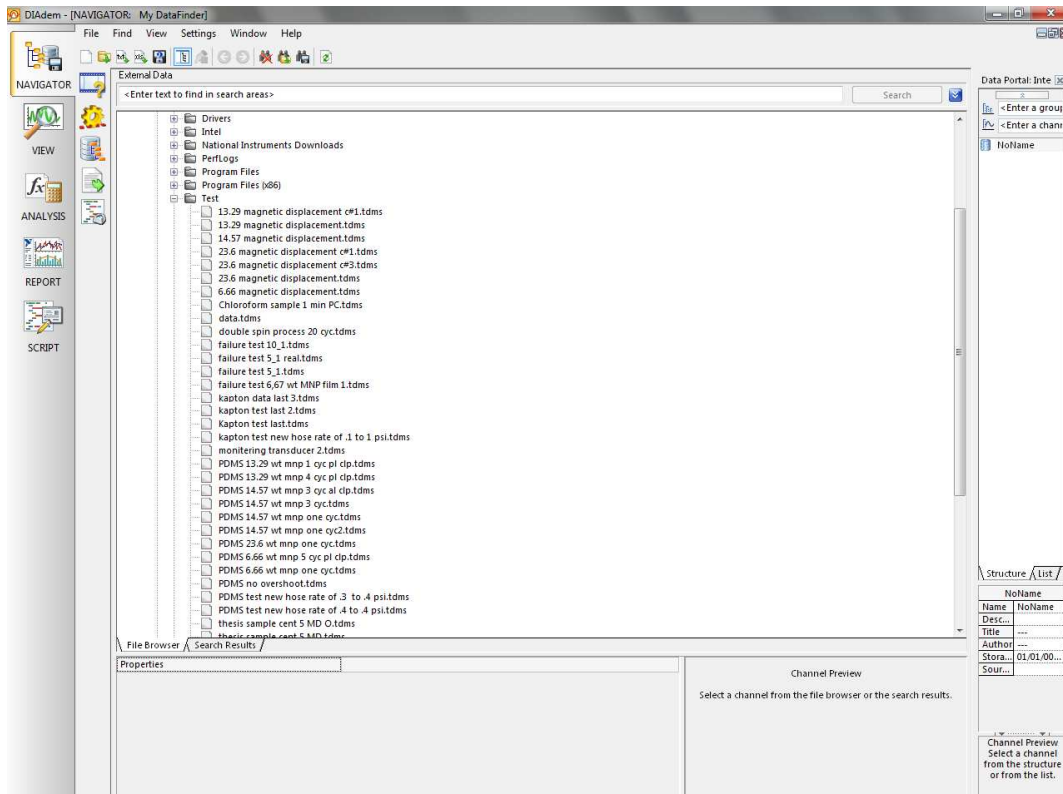


Figure A.5: DIAdem™ Software

Preparing Samples for Bulge Testing

- 1) Take one 1.7 cm² sample and flatten across the silicone mat reflective side down, ensuring no air is trapped between the interface to ensure that no buckling will be present during testing.

Note: Ensure that the mat is clean and free of dust.

- 2) On the bottom clamp add a thin glaze of superglue around the hole opening and quickly/carefully place on top of sample.

Note: It is better to perform this action on the air table that hosts the vibrometer apparatus, and be careful not to allow any glue too close to the hole opening.

- 3) Allow super glue to dry for two minutes and then gently pull away the silicone mat to expose sample surface.

Note: Be careful not to remove the mat impetuously, least damage to the metallic surface of the sample will occur.

- 4) Using the appropriate screws, attach the top clamp ensuring that it is flush with the bottom clamp.

Warning: Over tightening top clamp will result in presence of winkles across the sample surface and will be seen as overestimations in data evaluation.

- 5) Tightly screw clamped sample onto the testing stage.
- 6) Use stage micrometers to find the center of the sample.

Running Tests

- 1) Start the program by pressing the arrow button and change the desired parameters.
 - a) For bulge testing, change the precision, units, rate, rate mode, and set point to desired value.

Note: For magnet deflection, change precision and units only. Once the start button has been pressed, the program starts recording data

- 2) Apply parameters by pressing the control button.
 - a) If applying pressure cycles to the sample, then this program allows for negative and positive set points during a test.
- 3) When finished testing, press the control (measure) button and stop acquisition button.

Note: Magnetic deflection follows the same course of action except that the only buttons that need to be pressed to start and stop the data acquisition are the arrow and stop acquisition.

Turning Off the Bulge Testing System

- 1) Exit out of the DIAdem™ and LabVIEW program and shutdown computer.
- 2) Turn off laser and exit out of the MSA software.
- 3) Shutdown the computer, the MSA 400 vibrometer controller, the power source to the PMP 4060, the DPI 515, and the vacuum pump.
- 4) Close the air pressure valve.

A.3 References

- [A.1] Reid, Deformation and Adhesion of Thin Metallic Films on Flexible Substances, Materials Science and Engineering, Clemson University, (2011).
- [A.2] Druck DPI 515 Properties PDF, (2011).
- [A.3] GE Sensing PMP 4060 Properties, (2005).
- [A.4] Vlassak, New Experimental Techniques and Analysis Methods for the Study of the Mechanical Properties of Materials in Small Volumes, Stanford University, (1994).
- [A.5] Hohlfelder, Bulge and Blister testing of Thin Films and Their Interfaces ,Stanford University, (1998).
- [A.6] Small, Analysis of the Accuracy of the Bulge Test in Determining the Mechanical Properties of Thin Films, Journal of Materials Research, 7, (1992) 1553-1563.